MAPPING BEHAVIOURALLY INDUCED IMMEDIATE-EARLY GENE EXPRESSION ALONG THE SEPTOTEMPORAL AXIS OF CA1

SUTHERLAND THERESA ANN DUBE
Bachelor of Science, University of Lethbridge, 2012

A Thesis
Submitted to the School of Graduate Studies
of the University of Lethbridge
in Partial Fulfilment of the
Requirements for the Degree

MASTER OF SCIENCE

Department of Neuroscience
University of Lethbridge
LETHBRIDGE, ALBERTA, CANADA

MAPPING BEHAVIOURALLY INDUCED IMMEDIATE-EARLY GENE EXPRESSION ALONG THE SEPTOTEMPORAL AXIS OF CA1

SUTHERLAND DUBE

Date of Defence: December 14, 2016

Dr. B. L. McNaughton Supervisor	Professor	Ph.D.
Dr. R. J. Sutherland Thesis Examination Committee Member	Professor	Ph.D.
Dr. M. Mohajerani Thesis Examination Committee Member	Assistant professor	Ph.D.
Dr. R. Gibb Char, Thesis Examination Committee	Associate professor	Ph.D.

DEDICATION

To my family, for always making an effort (or at least pretending) to be interested in my work.

And to Richard, for your unending support throughout grad school. For words of encouragement, helpful discussions, and for gentle nudges when I'd get off track, I'm grateful.

ABSTRACT

The longitudinal (or septotemporal) axis of the rodent hippocampus is generally described as being functionally segregated. However, the division between septal and temporal areas is not clearly delineated, and current anatomic, genetic, and physiological data propose varying gradients and domains that in large part do not coincide**.** In an attempt to clarify these issues, we mapped the behaviourally induced activity of neurons throughout the longitudinal axis of CA1 using immediate early genes (IEGs), which enable large-scale analysis of neuronal activity at the cellular level with a high degree of spatial resolution.

Interestingly, the IEG data were not consistent with any of the proposed anatomical schemas or with the available single neuron recording data. The data suggest an alternative classification of hippocampal modules, with a functional domain in septal CA1 and a functional gradient through intermediate and temporal CA1. We suggest delineation between these two subdivisions of CA1 could correspond to amygdalar input to CA1. Further experiments could provide information on whether this input provides a basis for functional segregation at the level of neural activity dependent IEG expression.

ACKNOWLEDGEMENTS

First and foremost, I would like to thank my supervisor, Dr. Bruce McNaughton for his mentorship and guidance, and for providing me with the many opportunities he has to develop as a scientist. I would also like to thank the members of my supervisory committee, Dr. Robert Sutherland and Dr. Majid Mohajerani for their input and expertise. A special thanks to Dr. Francesco Battaglia and Dr. Tansu Celikel and their lab members for their support and technical expertise during my time at Radboud University Nijmegen. I would also like to acknowledge AIHS and NSERC for funding provided during my graduate program.

For technical assistance, I would like to thank the following people: Valerie Lapointe and Aubrey Demchuk for their help with perfusions, tissue preparation and tissue processing; Dr. Michael Eckert and Lilia Mesina for their image analysis scripts and expertise; Doug Bray and Dr. Maurice Needham for assistance with the microscopes; Dr. Isabelle Gauthier, Karen Dow-Cazal and the rest of the animal care staff; Behroo Mirza Agha for help with obtaining animals; and Amanda Mauthe-Kaddoura and Naomi Cramer for administrative assistance.

I would also like to thank the following past and present members of the CCBN for helpful discussions and advice throughout my graduate training: Wing Witharana, Dr. Zaneta Navrotilova, Megan Torry, Jeanne Xie, Victoria Holec, LeAnna Kalvi, Dr. Mariam Alaverdashvilli, Danielle Burger, Dr. Ben Clark, Hiroe Yamazaki, Adam Neumann, Dr. Dun Mao, Mitch Kesler, and Dr. Corinne Montes.

TABLE OF CONTENTS

LIST OF TABLES

LIST OF FIGURES

LIST OF ABBREVIATIONS

CA1: *Cornu ammonis* subfield 1
CA1d: dorsal CA1
CA1i: intermediate CA1
CA1v: ventral CA1
CA3: *Cornu ammonis* subfield 3
DAPI: 4'-,6'-diaminidino-2-phenylindole
DEPC: diethylcarbonate
DIG: Digoxigenin
DG: Dentate gyrus
EC: Entorhinal cortex
FISH: Fluorescence in situ hybridization
HC: Home cage
HRP: Horseradish peroxidase
IEG: Immediate-early gene
IP: Intraparotineal
MECS: Maximal electroconvulsive shock
mRNA: Messenger ribonucleic acid
NMDA: N-methyl-D-aspartate
PBS: Phosphate buffered saline
PCR: Polymerase chain reaction
PFA: Paraformaldehyde
RIO: Region of interest
RNA: Ribonucleic acid
SA: Streptavidin
TSA: Tyramide signal amplification
UTR: Untranslated region

CHAPTER 1: INTRODUCTION

The hippocampal longitudinal axis

The hippocampus' role in memory has been documented since the 1950's, following the use of medial temporal lobe lesions to relieve various neurophysiological and psychiatric disorders (Scoville, 1954; Milner and Penfield, 1955; Scoville and Milner, 1957). Later, the discovery of place cells in 1971 by O'Keefe and Dostrovsky led to the proposition that the hippocampus plays a vital role in memory through the creation of a cognitive map (O'Keefe and Nadel, 1978). In rodents, the hippocampus proper – consisting of the dentate gyrus (DG) and cornu ammonis (CA) – is a curved structure that spans most of the brain from the septal pole (dorsaomedial anterior areas) to the temporal pole (ventrolateral posterior areas). Current evidence suggests that there are functional differences in the way septal and temporal areas contribute to memory and spatial processing, however, these functional differences are not well understood.

While the firing characteristics of principal cells of hippocampal sub regions, mainly CA1, CA3, and the DG, have been relatively well characterized, functional differences along the septotemporal (longitudinal) axis have not been extensively explored. This difference is largely due to the difficulty in recording from or manipulating hard to reach temporal areas of the hippocampus. However, current evidence, based on connectivity, genetics, and physiology suggests differing functional sub-regions and/or gradients along the longitudinal axis of the hippocampus.

In much of the literature, the septotemporal axis is divided into three areas--septal, intermediate, and temporal--although this division is not clearly delineated (ex. Swanson & Cowan, 1977; Moser & Moser, 1998; Bast et. al., 2009). Generally, septal CA1 is

thought to be the center for cognitive functions, like spatial memory and navigation, whereas temporal CA1 is thought to contribute more to emotional or affective memories. Intermediate CA1 is generally thought of as being the graded area in between septal and temporal, receiving overlapping connections with both, and is commonly thought of as an interface for functions of septal and temporal regions.

In this thesis I utilize immediate-early genes to examine the relative differences in the proportion of active neurons along the septotemporal axis of CA1. Immediate-early genes (IEGs) such as *Arc* and *Homer1a* have been shown to be expressed in principal neurons in the hippocampus and elsewhere (Imamura et. al., 2011) and are expressed in approximately the same proportion of neurons in the hippocampus that have been reported to be active electrophysiologically (Guzowski et. al., 2006). Thus, we were able to characterize the proportion of IEG expressing neurons as a means to infer neural activation patterns with a high degree of spatial resolution, while also enabling the characterization of relative firing frequencies through the quantification of IEG expression, which has been demonstrated to correlate with place cell activity (Witharana, 2012).

Anatomy

Hippocampal neural circuitry, especially through the perforant path and so-called trisynaptic circuit (Anderson 1971), has been well established. For the most part, input to the hippocampus is directed from the cortex through superficial layers (II/III) of the entorhinal cortex to DG, then to CA3 and CA1 (and the subiculum), where input is then sent back through deep layers (V/VI) of the entorhinal cortex to cortical and subcortical

brain regions. However, there are strong, functionally significant cortical inputs from EC to CA1 (McNaughton et. al., 1989; Vago & Kesner, 2008), as well as from CA1 and the subiculum to the neocortex (Swanson, 1981; Jay & Witter, 1991; Parent et. al., 2010). In general, a regionally conserved pattern of connectivity is seen within the trisynaptic circuit in the transverse axis (Andersen et. al., 1971), however more divergent patterns of septotemporal connectivity are clear (Amaral & Witter, 1989).

Septal and temporal areas of the hippocampus show distinct differences in connectivity with other cortical and subcortical brain areas, strengthening the hypothesis that they are functionally distinct. These connections are mostly interposed through the EC, and are generally graded rather than discrete. Septal hippocampus generally receives more visuospatial inputs from areas like retrosplenial, occipital, postrhinal cortices through topographic projections from the dorsolateral EC (Dolorfo and Amaral, 1998; Fanselow & Dong, 2010; Strange et. al., 2014; Takata et. al., 2015). Temporal hippocampus, on the other hand, generally receives inputs from areas involved in affect regulation, such as prelimbic, infralimbic, and gustatory corticies, through ventromedial EC (Dolorfo and Amaral, 1998; Jones et. al., 2007; Fanselow & Dong, 2010; Strange et. al., 2014). The temporal hippocampus, especially CA1 and the subiculum, also receive direct input from the amygdala (Krettek & Price, 1977; Petrovich, Canteras, & Swanson, 2001).

These anatomical findings generally align with what would be expected given the results of lesion studies looking at the differing effects of disruptions to septal versus temporal hippocampus. These studies have generally (although not always) revealed that septal hippocampal lesions lead to deficits in spatial navigation memory, and temporal

lesions lead to deficits in memories related to fear and stress. For example, studies have shown that lesions restricted to the septal hippocampus reveal impairments in spatial navigations tasks such as the Morris water maze navigation task (Sutherland et. al., 1983) and that the extent of the lesion mirrors the extent of impairment on the task (Moser et. al., 1993; Moser et. al., 1995). Conversely, studies examining the effect of lesions to the ventral hippocampus generally report a disruption of affective characteristics, for example innate (Kjelstrup et. al., 2002) and learned (Hunsaker & Kesner, 2008) fear responses, such as exploration of open arms on an elevated plus maze or interruption of conditioned fear responses, respectively.

However, some lesion studies—particularly those examining the effects of lesions to temporal hippocampus—have produced varied results. One potential reason for this that is particularly relevant to the study at hand is that the delineations between septal and temporal hippocampus have not been clearly defined, and usually vary (Fanselow and Dong, 2010). Disparities in lesion site and extent may explain the mixed results when comparing some studies (Sutherland et. al., 2010). Additionally, the gradual differences in connectivity generally described by studies examining hippocampal connectivity along the septotemporal axis challenges the categorization of CA1 into discrete domains.

Physiology

Previous experiments looking at differences in neuronal activity along the septotemporal axis used electrophysiological recordings to reveal gradual differences in both the number of active neurons and the spiking activity of active neurons between septal and temporal CA1 (Jung et. al., 1994; Maurer et. al., 2005; Keinath et. al., 2014).

In septal CA1, there are more place fields, with cells showing smaller, more specific fields. In more temporal regions of CA1, fewer cells express fields in a given area, but fields are larger. Thus, septal place cells are thought of as having greater spatial 'resolution' than the cells in more temporal areas of CA1. It's important to note that while place fields in temporal CA1 are expanded compared with those in septal CA1, they do not overlap more; instead, it was found that overall there were fewer neurons with place fields in more temporal regions. Most of these studies, however, were limited to the septal and intermediate hippocampus, due to constraints in recording in far temporal areas of CA1. In CA3, recordings from along the entire extent of the axis have revealed an almost linear place field size gradient spanning the septotemporal axis (Kjelstrup et. al., 2008), corresponding to available data on CA1. However, the relative change in the population of neurons active was not explored in that study.

Place cell selectivity is hypothesized to be partially regulated by input from grid cells (cells in the entorhinal cortex that fire in a systematic, grid-like fashion (Hafting et. al., 2005)). Gradients in grid cell activity that provides input from entorhinal cortex (EC) to the hippocampus gives some possible insight into why this septotemporal difference in hippocampal place cell activity might be. As mentioned previously, more septal areas of hippocampus are connected with dorsolateral areas of EC, and more temporal areas of hippocampus are connected with ventromedial areas of EC (Dolorfo and Amaral, 1998; Strange et. al., 2014). Correspondingly, grid cells in dorsolateral EC show smaller spacing between grid fields as compared with grid fields in ventromedial EC (Stensola, et. al. 2012). This topographic pattern of connectivity is preserved through the trisynaptic circuit.

Another physiological difference between septal and intermediate/temporal CA1 is related to the increase of firing rate of place cells with running speed. It has been found that as an animal moves through a particular place field, the faster the pace the animal moves, the faster the firing frequency of place cell (Terrazas et. al., 2005; Maurer et. al., 2005). This variation in firing frequency with speed, however, is diminished in temporal hippocampus (Maurer et. al., 2005).

Precisely how these variations in neuronal activity along the septotemporal axis contribute to spatial navigation is not completely understood, however, data from all except one study are based on experiments recording from septal and intermediate hippocampus, due to technical challenges in recording from temporal areas. Information on more temporal areas, especially for CA1, could help elucidate how variations in activity along the septotemporal axis contribute to spatial navigation.

Gene expression

Through genetic analysis, CA1 has been recently been genetically categorized into three areas -- dorsal (CA1d), intermediate (CA1i), and ventral (CA1v) (Thompson, et. al. 2008; Dong, et. al., 2009). Based on in situ hybridization data of combined groups of genes from the Allen Brian Institute Atlas (Lein, 2007), these studies detailed not only molecular heterogeneity of cells along the septotemporal axis in CA1 and CA3, but also proposed discrete molecular domains (Thompson, et. al., 2008; Dong, et. al., 2009). In CA1, these areas were delineated based on specific expression boundaries for a number of genes combined for CA1d and CA1v, and a lack of expression of those genes for CA1i.

More recently, a study using next-generation RNA sequencing challenged the idea that CA1 could be genetically divvied up into discrete domains (Cembrowski, et. al., 2016). Their results indicate that there is pronounced variability in gene expression throughout CA1 (10-fold greater than what had been previously described), but did not align with previous findings indicating molecular subdivisions. They found many different genes enriched at either pole of the CA1, and a gradient of gene expression that was generally organized as a continuum between the septal and temporal poles. Importantly, the intermediate decay of gene expression between poles varied by individual gene. Although some genes exhibited sharper boundaries, the cutoff point septotemporally varied widely.

Interestingly, the examination of CA3 in this study confirmed previous findings that discrete genomic domains are present in this hippocampal subfield (Thompson et. al., 2009).

While the functional significance of heterogeneity in pyramidal cells is also not currently understood, the particular genes that were differentially expressed septotemporally include those involved in functionally significant processes, such as calcium signalling and synaptic transmission (Tushev & Schuman, 2016). Examining whether there are parallel physiological and molecular patterns across the septotemporal axis could likely provide interesting insights into the organization of CA1.

The hippocampal flat map

The difficulty in illustrating relative relationships of areas in the hippocampus was remedied with the development of the hippocampal flat map, which illustrated the entire hippocampal formation as a 2D schematic map (Swanson, Wyss, & Cowan, 1978). An example of the hippocampal flat map (an updated version from Petrovich, Canteras, and Swanson (2001)) is illustrated in figure 1.1. In order to display data from regions of interest (ROIs) along the septotemporal axis accurately and efficiently, in this study they are displayed on the flatmap of CA1.

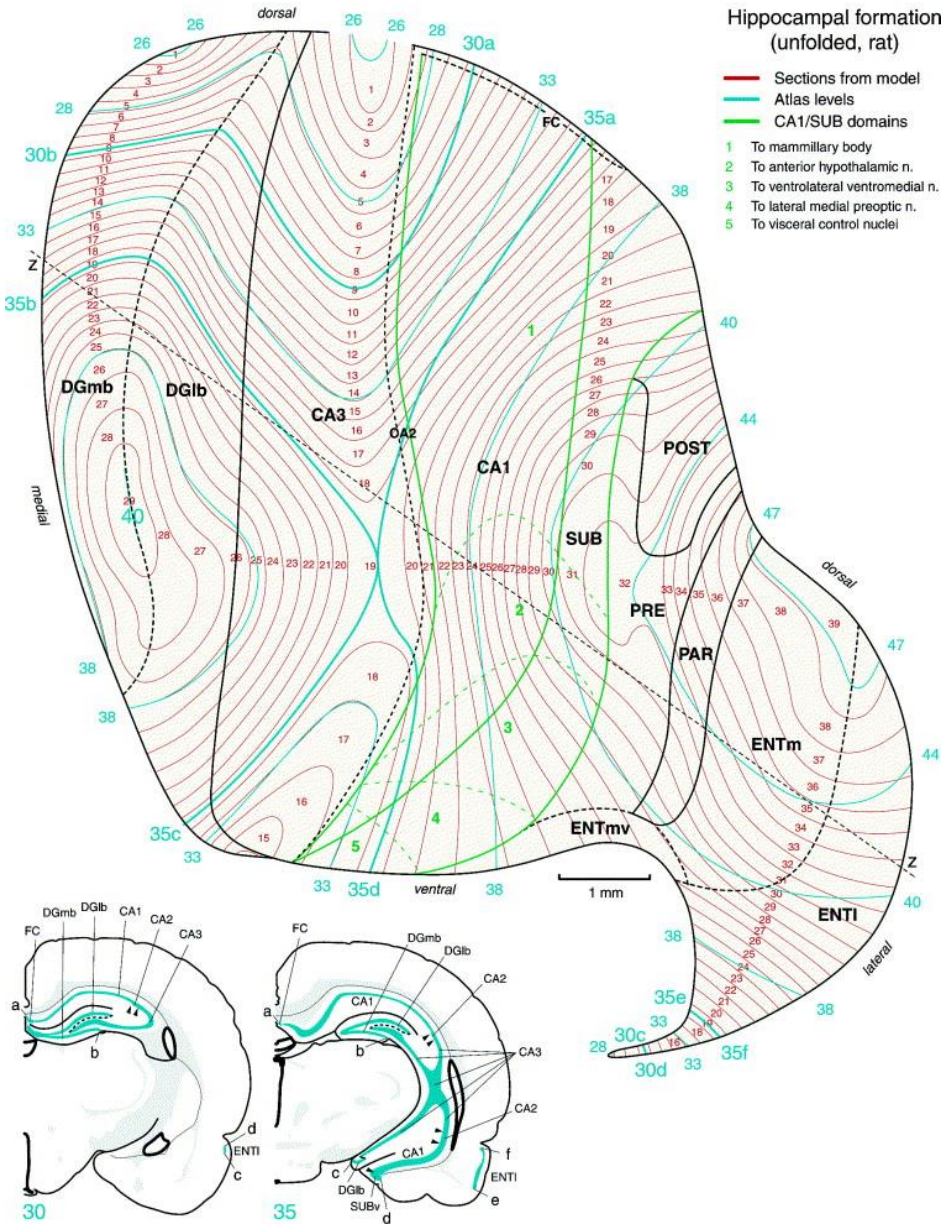

Figure 1.1. The hippocampal flat map. 2D schematic flatmap of the hippocampal structures and their relative locations. From Petrovich, Canteras, & Swanson, 2001.

Using immediate-early genes as markers of behaviourally induced neuronal activity

Immediate-early genes (IEGs), such as *Homer1a* and *Arc*, are transcribed rapidly and transiently following neuronal activity. These genes enable the characterization of active neurons through fluorescent detection of IEG mRNA, enabling large-scale analysis of neuronal activity at the cellular level (ex. Guzowski, 2002; Guzowski et al, 2005; Chalwa et. al., 2004), with a high degree of spatial resolution.

Traditional notions of eukaryotic mechanisms of transcription initiation (i.e. a polymerase locating promoter regions, binding DNA, recruiting transcription factors to the promoter region etc.) are still prevalent. However, evidence has shown that it's more likely that RNA polymerase II (RNAPII) (the polymerase responsible for transcribing mRNA) transcribes genes in stable units termed transcription factories (ex. Iborra,et. al., 1996; Sutherland & Bickmore, 2009; Mitchell & Fraser, 2008). These transcription factories create localized mRNA clusters that appear as intranuclear transcription foci (INF), or 'blobs'. While the conventional method of characterizing IEG blobs is Boolean (i.e. present or not present, corresponding to a neuron being active or not active, respectively), several previous studies suggest that blobs size and intensity characteristics may correlate with mRNA levels (Penner et al., 2011) and in turn this may correlate with the total spike activity of neurons over a certain temporal window (Miyashita et al., 2009; Witharana et. al., 2012). Indeed, it has recently been demonstrated that INF integrated intensity for the IEG Homer1a corresponds to increases in place cell activity (Witharana, 2012; Witharana et. al., 2016).

Studies looking at the transcription of neuronal IEGs have revealed that some, such as *Fos* and *Junb*, contain upstream depolarization-dependent transcriptional

regulatory Short Interspersed Elements (SINEs) that chaperone the relocation of IEGs to transcription factories following neuronal activity (Crepaldi et. al., 2013). Others, such as *Arc* and *Egr1*, are continuously poised at transcription factories with multiple RNAPIIs bound (Saha et. al., 2011). In this case, it has been demonstrated that following neuronal activity even more RNAPIIs are recruited and begin to transcribe the IEG (Saha et. al., 2011), supporting the idea that multiple spikes can produce bursts of increasing amounts of mRNA that can then be quantified. However, the precise stoichiometric relationship between spiking activity and the expression of these genes has yet to be determined.

Because previous studies have already correlated increasing blob size and intensity with spiking activity using *Homer1a* (Withawana et. al., 2012), we have chosen to use this IEG in the current study (along with *Arc* for positive control animals). *Homer1a* is an alternatively spliced isoform of constitutively expressed Homer1b and Homer1c proteins (Bottai et. al., 2002). While Homer1b and Homer1c act as scaffolding proteins to facilitate interactions between metabotropic glutamate receptors and downstream effector proteins, *Homer1a* competitively binds these proteins, but lacks the domain to facilitate coupling (Kammermeier & Worley, 2007; Shiraishi-Yamaguchi & Furuichi, 2007). Thus, the main role of *Homer1a* in neurons is to maintain homeostatic synaptic scaling, which is a form of neuronal plasticity that maintains homeostasis in neural networks despite changes in activity (Hu et al., 2010).

The home cage question

With the advent of automated detection and characterization of IEG blobs, a higher number of IEG positive neurons than predicted have been detected in home cage (HC) control animals, reaching levels near those of behavioural animals (Witharana et al., 2016). Detailed analysis of these foci in the hippocampus have revealed that small, dim foci are present in HC animals, whereas brighter, larger blobs (as measured by integrated intensities) along with smaller, dimmer foci, are present in behavioural animals (Witharana et al., 2016). The bimodal distribution of behavioural animals presents the question of whether smaller, dimmer foci are perhaps blobs induced by exploration of the home cage, rather than representative of the behavioural task.

In an attempt to reduce the possible home-cage blob contamination in this experiment, we continued the behavioural task throughout the time-course for *Homer1a* gene induction, rather than returning the animals to the home cage after the usual 5 minutes of a behavioural task. Previous unpublished results in our lab have characterized the expression of *Homer1a* over time from 2 to 50 minutes post-induction (figure 1.2). We found that blobs began to appear at about 20 minutes following induction. Area-normalized blob numbers peaked at about 28-34 minutes, but remained high until after 40 minutes, although these figures varied slightly depending on the method of imaging and blob quantification. In all cases, however, the number of blobs began decreasing in number by 42 to 50 minutes. From this timeline it is estimated that *Homer1a* mRNA likely diminishes from the nucleus by approximately 25-30 minutes following peak induction. Therefore, in order to ensure any home cage *Homer1a* expression was

diminished in behavioural animals, the behavioural task in the current study lasted 36 minutes.

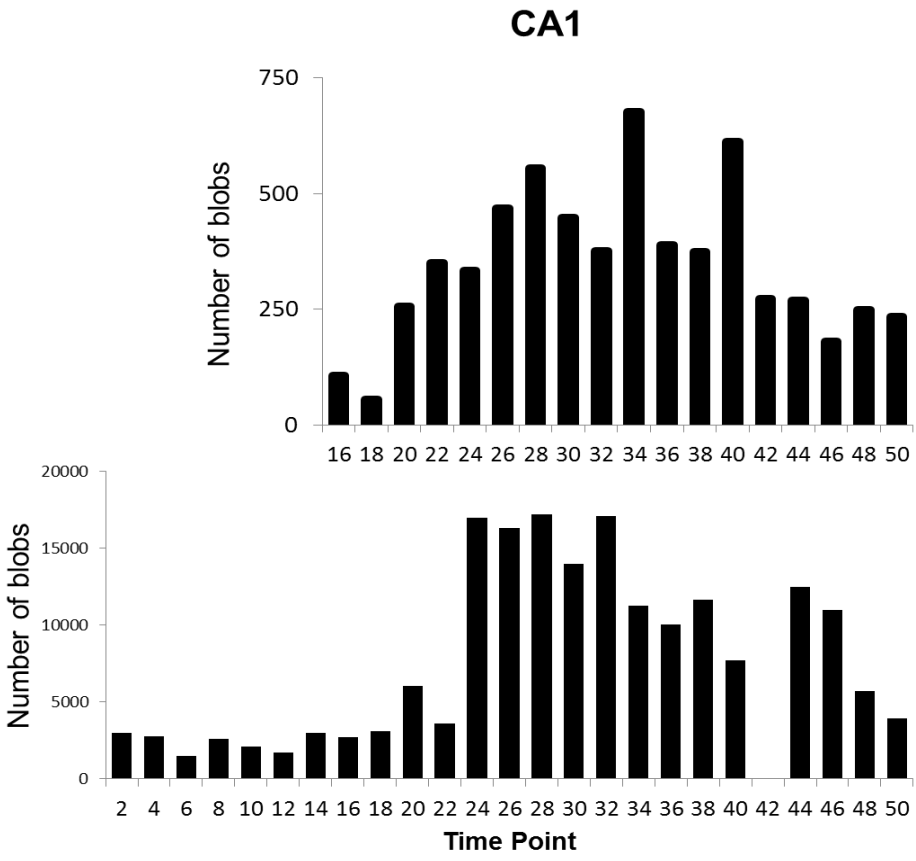

Figure 1.2. *Homer1a* time course analysis data detailing the relative number of blobs over time. Time course data was based on MECS IEG induction. Top: Confocal analysis of blobs over time from 16 to 50 minutes. Bottom: NanoZoomer analysis of blobs over time from 2 to 50 minutes.

Present study predictions

In this study we mapped the behaviourally-induced transcriptional activity of neurons throughout the longitudinal axis of CA1 using IEGs, which enabled large-scale analysis of activity at the cellular level with a high degree of spatial resolution. Based on previous electrophysiological findings, we predicted that the proportion of IEG+ nuclei would decrease from septal to temporal CA1 (figure 1.3). We also predicted that, because place cells in temporal CA1 have larger fields than place cells in septal CA1, the mean IEG expression quantified within IEG+ nuclei would be greater in temporal as opposed to septal CA1. We expected that these predictions would be reflected in the sparsity of the overall distributions of fano factor values (calculated using: $\text{mean}(x)^2/\text{mean}(x^2)$, where x is the fano factor value of each nucleus), with sparsity values expected to be higher in septal and lower in temporal CA1.

Additionally, based on the time-course of the behavioural task and the approximate decrease in *Homer1a* mRNA within the nucleus following peak induction, we expected that the relatively high proportion of blobs found in home cage controls would be diminished in the current study.

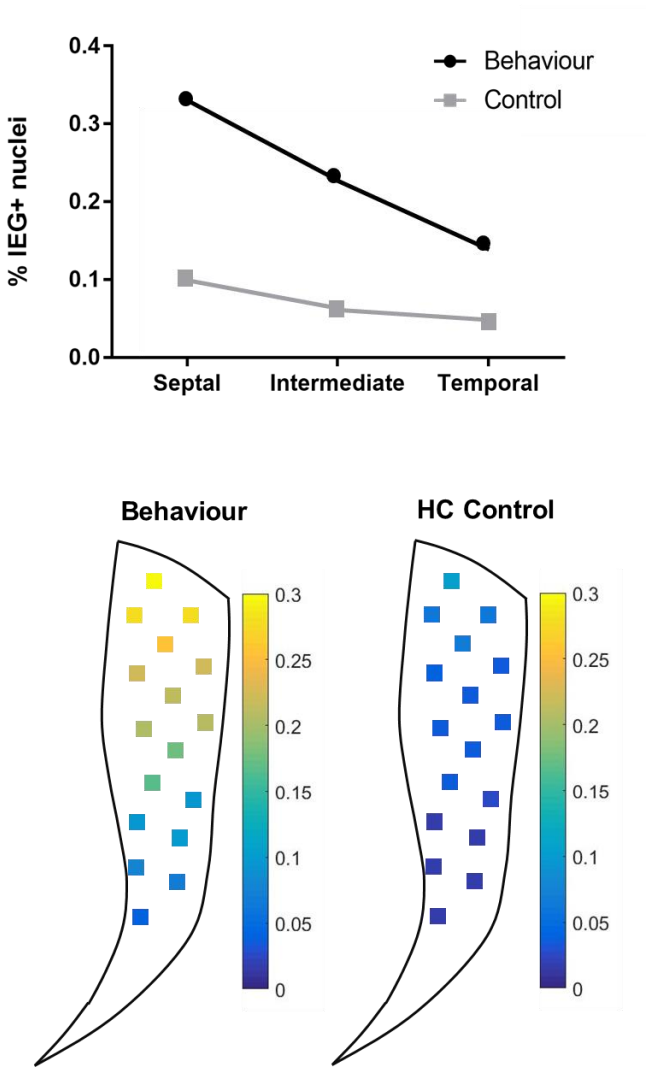

Figure 1.3. Predicted trends in Homer1a expression. Top: Predicted trend in the proportion of IEG+ nuclei in septal, intermediate, and temporal CA1. Bottom: Hippocampal flat map visualization of the predicted proportion of IEG+ nuclei throughout CA1.

CHAPTER 2: METHODS

Subjects and handling

Thirteen mice (C57 background, 3-6mo.) were housed in pairs or triplets on a twelve-hour light/dark cycle, with food and water available *ad labium.* All procedures were performed in accordance with the Canadian Council on Animal Care and University of Lethbridge Animal Welfare Committee guidelines.

Each mouse was handled for approximately 5 minutes daily in the home cage room for 7 days prior to behavioural testing. Three days prior to testing, mice were separated and housed individually. On testing day, mice were randomly assigned to one of three groups: behvaioural exploration (n=6), home cage control (n=6), and positive control (maximum electroconvulsive shock (MECS)) (n=1).

Behavioural testing

On testing day, animals in the behavioural exploration group were placed in a transport cage in the housing room, covered, and transported to the behavioural room located approximately 10m away from home cage room. Mice were placed into a circular behavioural arena containing a 3x3grid (made with masking tape), with visual cues on the wall of the room and in the arena, and dim lighting. Animals were allowed to explore the behavioural arena for 36 minutes, with the experimenter ensuring that the animal transversed each grid approximately equally throughout the exploration time. If the animal did not move itself, the experimenter placed the animal into a different grid. Following the 36 minutes of exploration, animals were transferred to a perfusion room for immediate sacrifice. Animals in the home cage group were taken straight from the

home cage room to the perfusion room to be sacrificed. Animals in the positive control group received maximum electroconvulsive shock (MECS) in order to induce IEG expression, left in a covered transport cage for 36 minutes, then sacrificed. MECS parameters were as follows: 60 pulses at 04 ms for 02 seconds and 75mA.

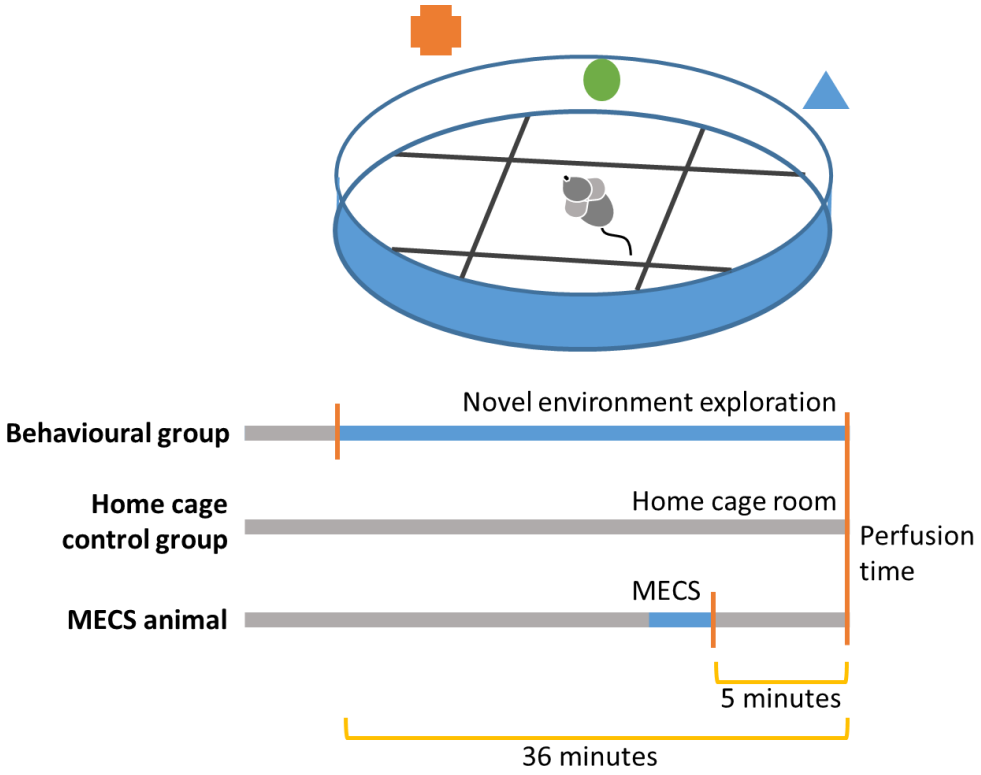

Figure 2.1. Timeline for the induction of IEGS in behavioural, home cage control, and MECS control groups. In the behavioural group (n=6), animals explored a novel environment for 36 minutes to correspond with the induction timeline of *Homer1a*. The home cage control group (n=6) were taken straight from the home cage room and perfused. The positive control animal (n=1) received MECS to induce the expression of *Arc* and was 5 minutes following induction. Figure not to scale.

Sacrifice and Tissue Preparation

Animals were placed in an isofluorane chamber until fully anesthetized immediately upon entry to the perfusion room. Animals then received an intraperitoneal (IP) injection of 0.1-0.25mL of Euthansol (sodium pentobarbital). Once deeply anesthetized, animals were perfused intracardially with RNAse free 1X phosphate buffered saline (PBS) followed by 4% paraformaldehyde (PFA). Brains were extracted and placed into 4% PFA for 2 hours, then placed in a 30% sucrose solution until sunk (approximately 1.5 days).

Following cryopreservation, brains were cut down the midline to separate hemispheres. Brains were then flash frozen using dry ice and ethanol, then embedded in OCT and stored at -80°C. The left hemisphere of each mouse brain was then cut on a coronal plane at 40μm/section using a cryostat. Sections were placed in wells containing 1X PBS and mounted on Superfrost Plus slides, dried and stored at -80°C.

Fluorescence in situ Hybridization (FISH)

Homer1a and *Arc* FISH was performed as previously detailed (Guzowski et. al, 1999; Montes-Rodriguez et. al., 2013; Witharana et. al., 2016). Briefly, DIG labelled antisense riboprobes probes targeting the 3' untranslated region (UTR) of mouse *Homer1a* and intronic sequences of *Arc* mRNA were synthesized using polymerase chain reaction (PCR) and in vitro transcription.

Slides stored at -80°C were thawed completely, and then incubated in 4% PFA (4°C) for 4 minutes, followed by a 2 minute wash in 2xSSC to remove residual PFA. Slides were then incubated with proteinase K (3ul in 1 mL proteinase K buffer per slide)

for 30 minutes in order to increase tissue permeability. Again, slides were fixed in 4% PFA for 3 minutes, and then washed in 2X SSC. Following a 10 minute incubation in acetic anhydride (in order to increase probe binding specificity), slides were rinsed in DEPC treated water and incubated in a 1:1 acetone/methanol solution for 5 minutes at -20 to remove lipids from tissue. After an additional wash (5 minutes) in 2X SSC, slides were incubated in pre-hybridization buffer for 1 hour to increase probe binding specificity. Slides were then incubated in 3ng/µl of probe in hybridization buffer overnight (approximately 16 hours) at 56°C.

Following the overnight incubation, slides were left to cool to room temperature and washed several times in 2X SSC to remove residual hybridization buffer and probe. Slides were then washed in an RNAse a solution for 30 minutes at 37 °C to destroy any remaining single stranded RNA, then washed in 2X SSC and 0.5X SSC. Following a 30 minute incubation in 2%H_2O_2 (to quench any endogenous peroxidases that may interfere with the antibody-HRP specificity in binding to TSA-biotin), slides were washed in TBST for 10 minutes and incubated overnight (approximately 16 hours) with HRP conjugated anti-DIG.

After the overnight antibody incubation, slides were washed several times in TBST, and incubated for 60 minutes with tyramide conjugated biotin. The tyramide targets and binds to the HRP conjugated ant-DIG, providing signal amplification. Following several washes, slides were then incubated with a streptavidin (SA) -Texas red conjugate for 30 minutes, to bind biotin and provide a fluorescent marker. Slides were again washed several times with TBST then with TBS, and counterstained with DAPI,

which enables visualization of neuronal nuclei. Vectashield was used for cover slipping and slides were then sealed with nail polish.

Imaging

The entirety of each slide was initially imaged using a NanoZoomer (Hammamatsu) digital microscope for detailed large-scale visualization of each series of brain section. Next, tiled z-stacks of CA1 were imaged using a laser scanning confocal microscope (Olympus Fluoview 1000). Each z-plane had a step size of 0.5µm and a depth of 18µm (37 stacks per image). Further details on NanoZoomer and confocal imaging can be found in appendix A.

Regions of Interest

The regions of interest (ROIs) consisted of the entire CA1 layer imaged in even intervals from anterior to posterior. Five sections, each approximately 480um apart, were used for each brain covering septal to temporal CA1. Images of each section were first cropped to exclude nuclei outside of the CA1 layer, then multiple square RIOs were segmented as shown in figure 2.2. In total, 17 ROIs were used, labelled A-Q, and overlaid on the hippocampal flat map based on their position along the septotemporal axis of CA1 (as shown in figure 2.2).

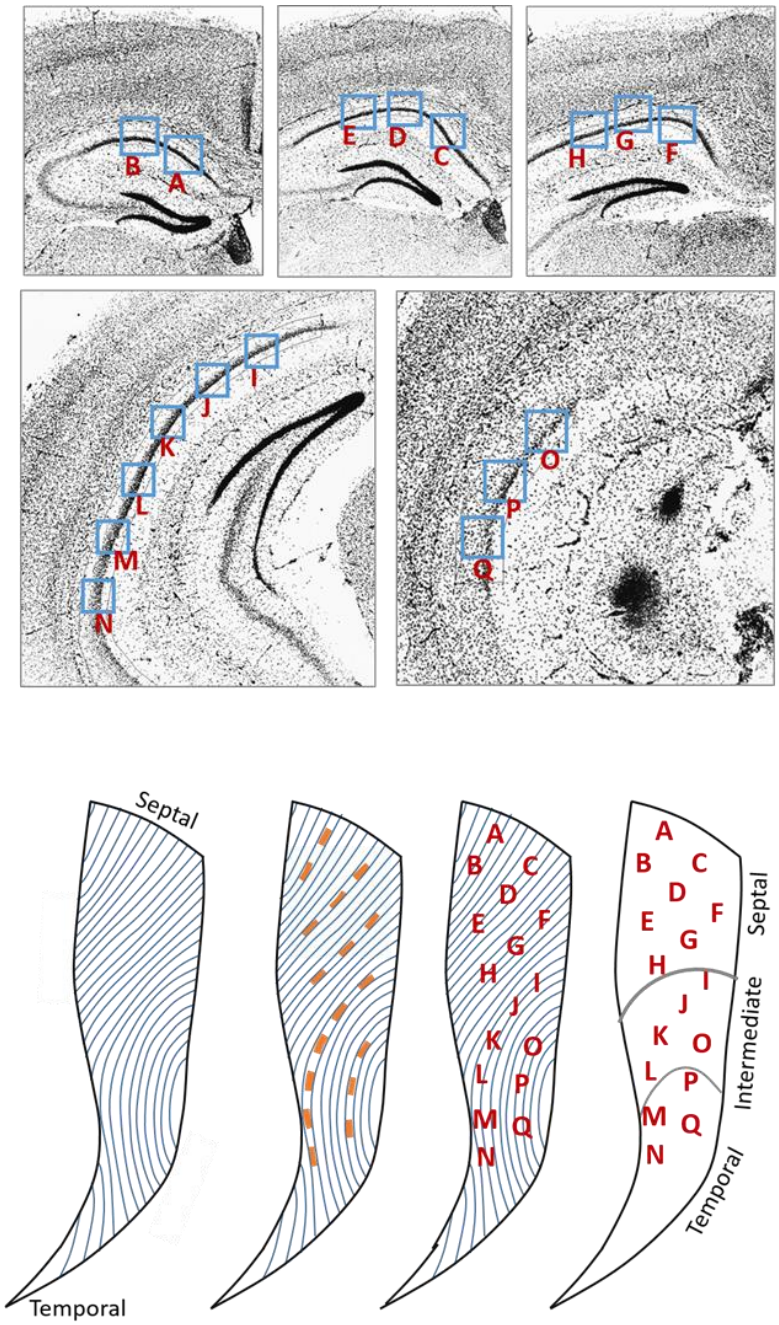

Figure 2.2. Regions of Interest along the septotemporal axis of CA1 and their relative positions on coronal sections and the CA1 flatmap. Top: ROIs from CA1 were imaged using a confocal microscope. Square ROI subregions were segmented from along the septotemporal axis (A-Q). Bottom: Following analysis, IEG data from each subregion was compiled according to position from the septal to temporal pole and overlayed on the hippocampal flatmap of CA1, and delineated into septal, intermediate, and temporal.

Image Analysis

Automatic analysis of DAPI – stained nuclei and fluorescent IEG foci was performed using a number of programs. Together, these programs enabled the analysis of blob features (such as the number of blobs, the integrated intensities of each blob, and their position in the image), as well as the identification of their corresponding nuclei. This enabled analysis that combined blob features with nuclear features such as fano factor, average pixel intensity and total integrated intensity.

Automated blob detection and quantification

A Java based ImageJ plugin (IEG Analysis, V. Trivedi) was used to automatically analyze tiled image stacks for characteristics of individual blobs in 3D space using user specified parameters (see table 5.1, appendix A, figure 2.3). Methods for detecting blobs have been detailed previously (Montes-Rodriguez et al., 2013; Du et al., 2011). Briefly, blobs were defined by local maxima and expanded until pixels no longer reached the user specified thresholds for either the blob itself or the nuclear background (in order to decrease the detection of 'blobs' that were not located inside of a nucleus). All continuous pixels that met those thresholds were included in the blob initially. Following this step, each blob was accepted or rejected based on user defined input parameters, such as size and peak thresholds. A final list of all remaining blobs and their associated features was output. Blob features quantified included number of blobs, position of each individual blob, and integrated intensity and size of each blob.

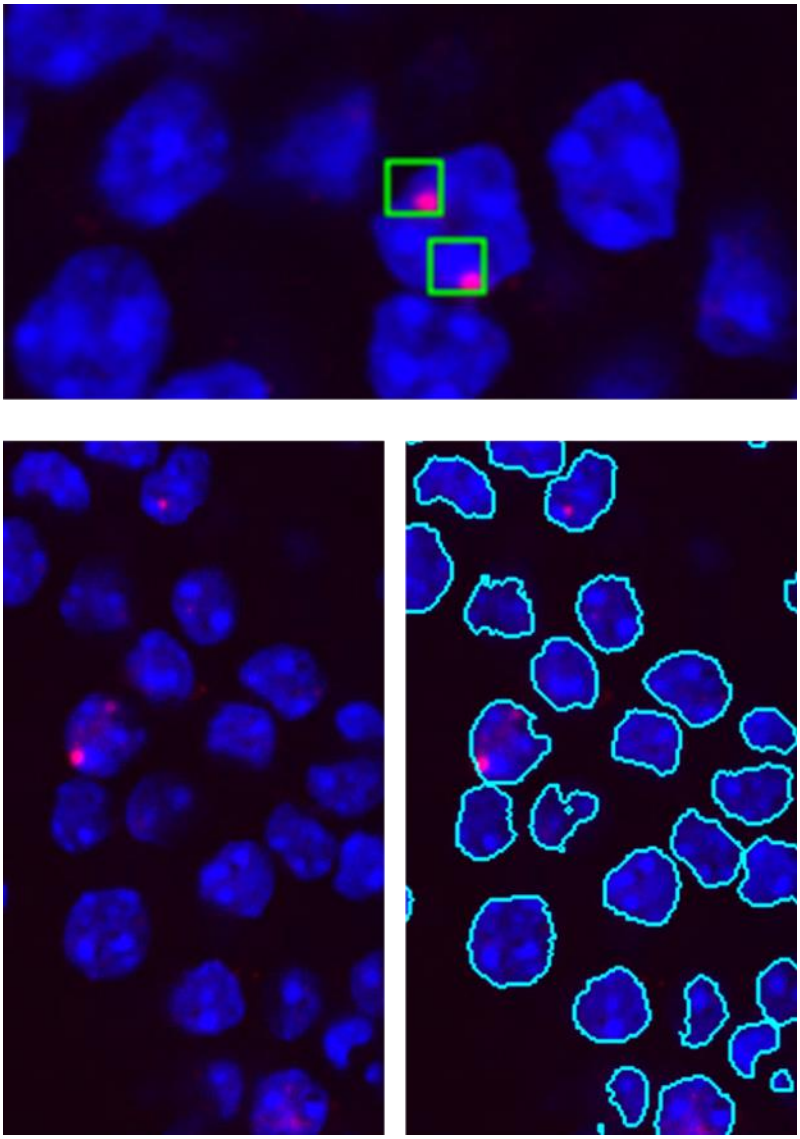

Figure 2.3 Example of blob detection and FARSIGHT nuclear segmentation. Top: single layer confocal image with blob detection and identification using IEG Analysis. Bottom: Single layer confocal image with example showing the raw image (left), and the image with nuclear boundaries superimposed (right).

Nuclear Segmentation

Following blob detection, automated 3D nuclear segmentation on confocal z-stacks was performed (figure 2.3). Images were first preprocessed using ImageJ, which involved splitting colour channels. To the blue channel, a median blur of 3 pixels (to reduce high frequency noise) and a contrast stretch was applied. Next, nuclear boundaries were automatically detected and delineated with FARSIGHT, an open source program that has been described in detail and verified elsewhere (Bjornsson et. al., 2008; Al-Kofahi et. al., 2010; Wilber et. al., 2015). Preprocessing and segmentation were performed using a Matlab interface batch script (runBatchMode, L. Mesina). All nuclei were subjected to a volume threshold of 5619-10645 (the mean volume value +/- 0.75 standard deviations) pixels and images were guard zoned 10 z-stacks from the top and bottom of the image stack and 30 pixels from the edges.

Using borders of segmented nuclei overlaid on the original confocal images, details about pixel intensity and variation were characterized as an indication of IEG expression (Blobless analysis, M. Eckert). Many characteristics were quantified for each nucleus, but only average intensity and fano factor were used in the current analysis. The average was calculated as the mean intensity values for all pixels within the nuclear boundaries for a specific colour channel corresponding to the stain for the IEG of interest (in this case, red). Average red was used as a measurement to quantify the mRNA throughout the nuclei, instead of just mRNA localized to blobs. The fano factor was calculated as the pixel variance in each nucleus divided by the mean, and gave an indication of whether the distribution of red pixels within a nucleus was concentrated in a

relatively small proportion of pixels. The fano factor measurement provided a method to quantify the tendency of the mRNA to be localized into blobs (figure 2.4). In addition to these measurements, this script enabled the overlay of blob coordinates so nuclear features could be directly compared with blob features characterized using IEG Analysis.

Statistics

For results grouped into septal, intermediate, and temporal areas, a repeated measures ANOVA was used to calculate statistical significance based on the average proportion of IEG+ nuclei for each animal in each subregion (repeated measures were based on proportions for septal, intermediate, and temporal for each individual animal). A post-hoc Holm-Siddak test was then done for multiple comparisons. For fano factor analysis, IEG+ nuclei were defined as those having a fano factor value of 2 standard deviations above the home cage mean. For blob analysis, IEG+ nuclei were defined as those containing at least one blob. For results based on distributions of quantified IEG expression, a two sample Kolmogorov-Smirnov test was done. Figures for these distributions were normalized and smoothed based on a probability density function (so that the area under the curve summed to one), using ksdensity in Matlab.

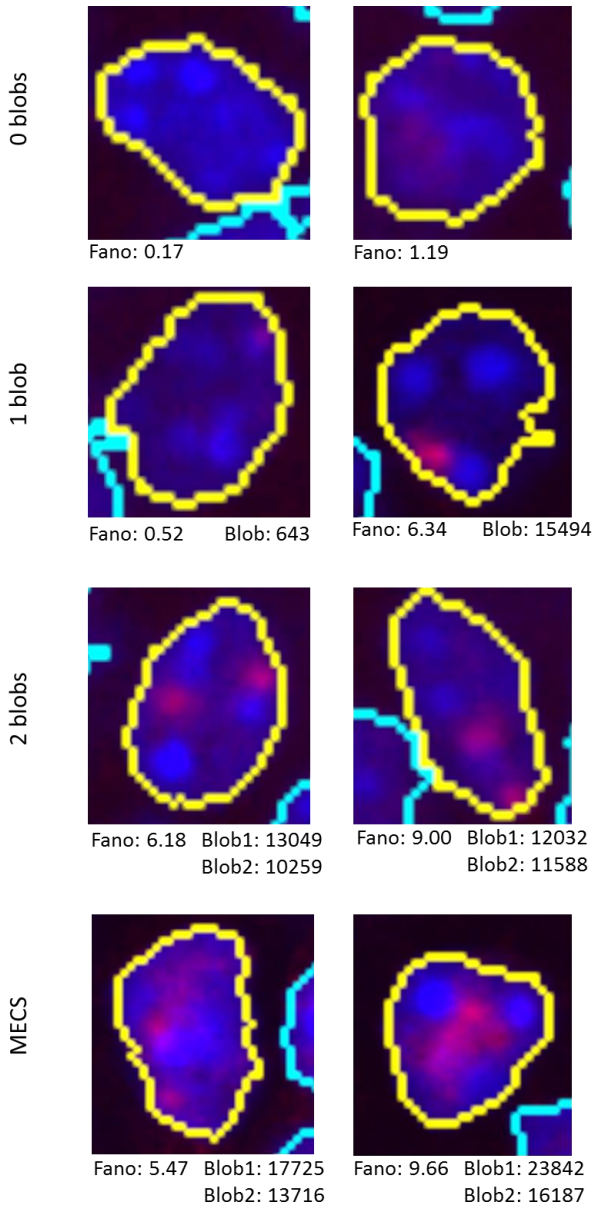

Figure 2.4. Comparison of fano factor values with blob integrated intensity values. Fano factor values from segmented nuclei (yellow boundaries) and total integrated intensity values from blobs within the nuclei are listed below each nucleus.

CHAPTER 3: RESULTS

IEG expression was measured in nuclei from various positions along the septotemporal axis

Following guard zone and nuclear volume exclusions, a total of 30,125 nuclei were sampled from all animals in all conditions. From this, approximately half were from the behavioural condition and half were from the home cage control condition. Table 3.1 presents a summary of the numbers of nuclei sampled from dorsal, intermediate and temporal areas for behavior, HC control, and MECS control conditions. Seventeen positions were sampled along the septotemporal axis at various positions on the hippocampal flatmap.

Table 3.1 Number of nuclei sampled from septal, intermediate, and temporal positions in CA1 in behavioural, home cage control, and MECS control conditions.

	Behaviour (# nuclei)	Home cage control (# nuclei)	MECS control (# nuclei)
Septal CA1	6542	6198	1091
Intermediate CA1	4274	4533	677
Temporal CA1	3046	3258	506

Novel environment exploration induced IEG expression

Overall, the distribution of fano factor and average red values in the behavioural condition was right shifted compared to that of the home cage (figure 3.1), with the behavioural condition showing a greater number of nuclei expressing a greater amount of IEG (as indicated by fano factor and average red value) as compared to the home cage condition. In order to classify nuclei as IEG+ or IEG- using fano factor, we used 2 standard deviations above the mean of the home cage control group as a threshold. Nuclei with a fano factor value higher than the threshold were classified as IEG+. During the behavioural exploration task, each animal transversed each grid an average of 182 times in the first 20 minutes of behavior. During this time, animals were moved to different grids by the experimenter an average on 36 times each.

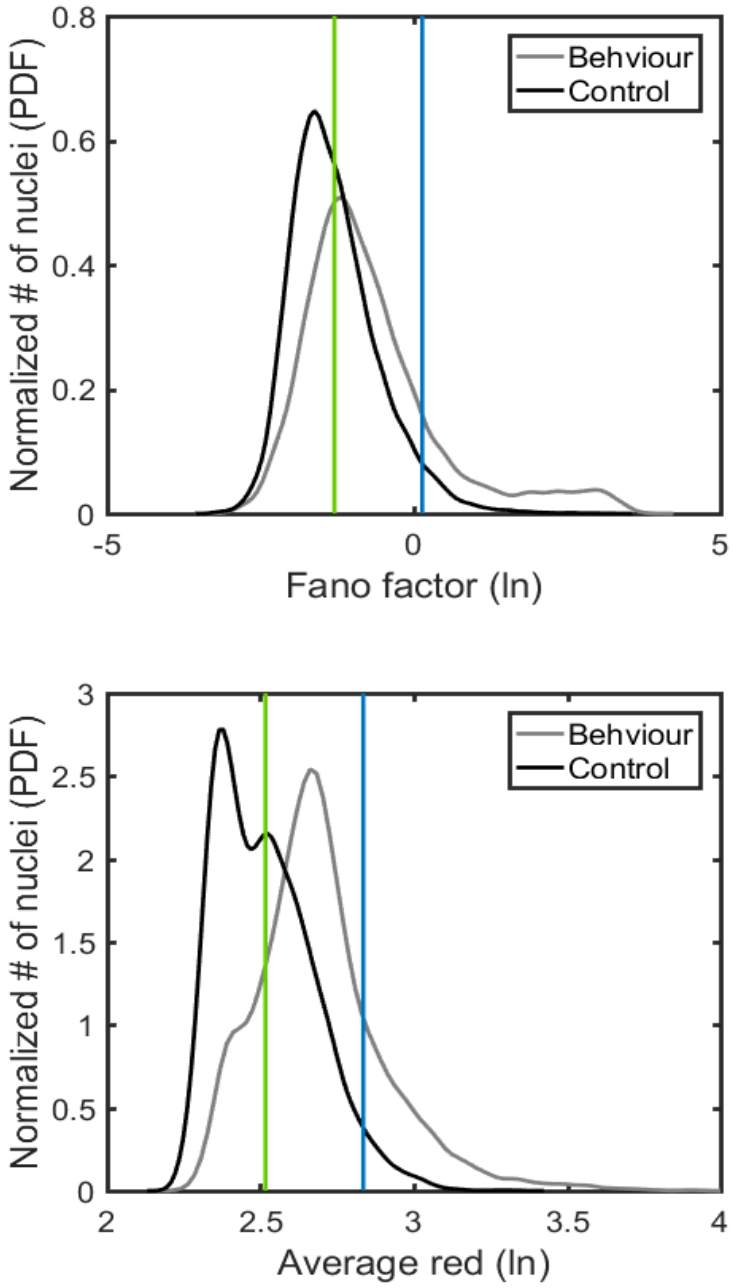

Figure 3.1. Normalized distributions of fano factor values (top) and average red (bottom) from nuclei in home cage control and behaviour animals. Green vertical lines represent the home cage control mean, and the blue lines represent 2 standard deviations above the home cage control mean. IEG+ nuclei were defined as those nuclei having a fano factor value exceeding the threshold of 2 standard deviations above the home cage control mean value. These values are as follows: Fano (ln) Mean = -1.2928, STD = 0.7157, Mean + 2 STD = 0.1387; Average (ln) Mean =2.5167, STD = 0.1592, Mean + 2 STD = 2.8351.

Proportion of IEG+ nuclei in septal, intermediate, and temporal areas

The proportion of neurons classified as IEG+ in the behavioural exploration condition was significantly greater than those in the home cage control condition, and this was the case for each of septal, intermediate, and temporal areas ($p<0.0001$, $p=0.0173$, and $p=0.0110$, respectively) (Figure 3.2).

The average proportion of IEG+ nuclei was 23% in septal areas, 11% in intermediate areas, and 18% in temporal areas. There was no significant difference in IEG+ nuclei between septotemporal areas within the home cage-control animals ($p>0.05$ for all comparisons). In the behavioural group, there was a significant difference in the proportion of IEG+ nuclei between septal and intermediate areas ($p=0.0018$), but not between septal and temporal ($p=0.0795$) or intermediate and temporal ($p=0.0795$) (figure 3.2).

Proportion of IEG+ nuclei overlaid on the hippocampal flatmap

In order to determine the relative septotemporal and proximodistal position of each area sampled, we overlaid each ROI with its corresponding position on the hippocampal flatmap (see figure 1.1, figure 2.2), with each ROI represented as a square on the flatmap (figure 3.3). For each square, we calculated the proportion of IEG+ nuclei, and created a heatmap based on those values. The colour of each square relative to its corresponding colourbar represents the proportion of IEG+ nuclei in that specific position of CA1.

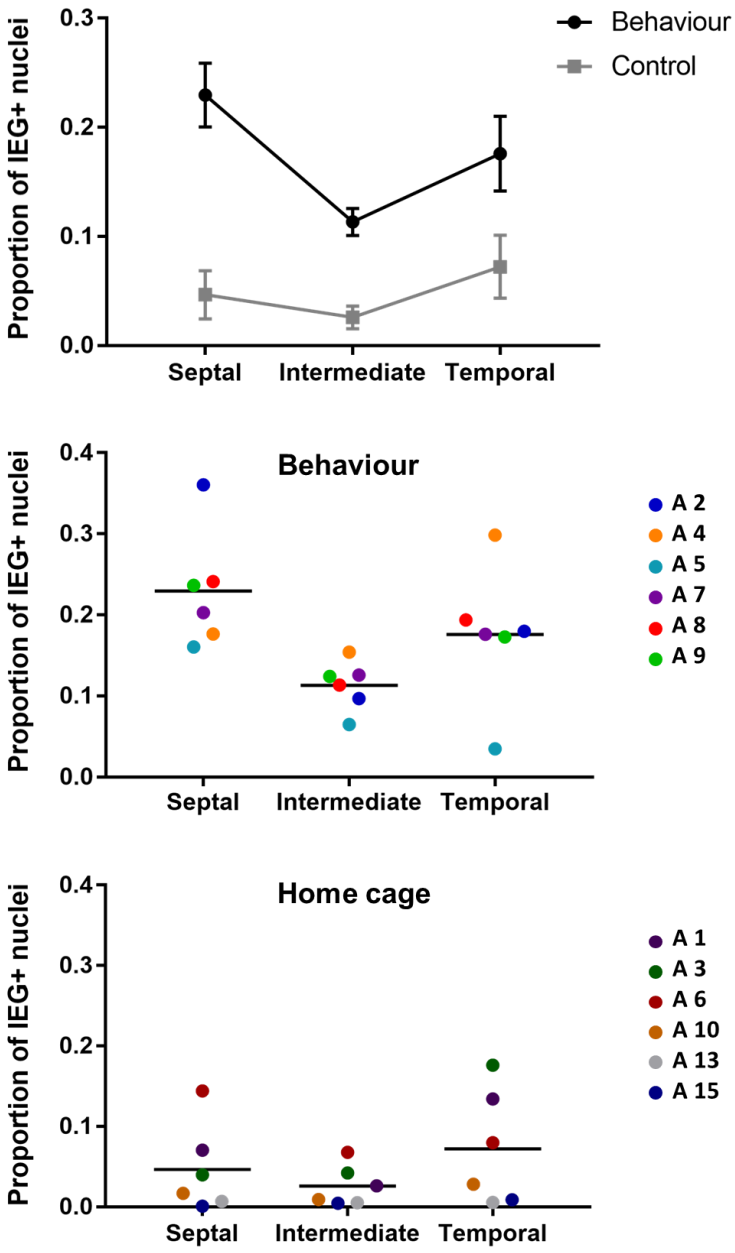

Figure 3.2. Average proportion of IEG+ nuclei in septal, intermediate, and temporal CA1 in control and behavioural groups. IEG+ nuclei are defined as those nuclei having fano factor values exceeding the threshold of 2 standard deviations above the home cage control mean fano factor value. Top: Comparison of proportion of IEG+ nuclei between behaviour and control animals in septal (p<0.0001), intermediate (p=0.0173), and temporal (p=0.0110) CA1. Comparisons of proportion of IEG+ nuclei within groups between septal, intermediate, and temporal were as follows: Behaviour -

Multiple comparisons reveled a significant difference in septal vs. intermediate (p=0.0018), with no other comparisons reached statistical significance (septal vs. temporal (p=0.0795); intermediate vs. temporal (p=0.0795)). Control - No comparisons reached statistical significance (septal vs. intermediate (p=0.6164); septal vs. temporal (p=0.6164); intermediate vs. temporal (p=0.3204)). Statistical comparisons were two-way repeated measures ANOVA, with a post-hoc Holm-Siddak test for multiple comparisons. Middle, bottom**:** Proportion of IEG+ nuclei in septal, intermediate, and temporal CA1 by animal. Lines indicate means. Dots represent values for each animal, with colour identifying individual animals across regions. Error bars represent SEM.

Proportion of IEG+ nuclei by septotemporal position

In order to determine the proportion of IEG+ nuclei in order from septal to temporal poles, each ROI was arranged based on its relative septotemporal position on the CA1 flatmap, disregarding its proximodistal position (figure 3.4). This data revealed a consistently high proportion of nuclei were IEG+ in approximately the septal half of CA1, with an average of 23%. In the temporal half of CA1, the average proportion of IEG+ nuclei was 13%; however, the values of individual ROIs dropped off sharply to just 7% in the ROI closest to the septal half, but showed a graded, stepwise increase to over 20% of IEG+ nuclei in the most temporal areas of temporal CA1. In general, these trends were mirrored in the home cage control animals, but with an average of 5% of IEG+ nuclei in the septal half, and 4% in the temporal half. The gradual increase in the proportion IEG+ nuclei in temporal areas was less obvious in the home cage control group.

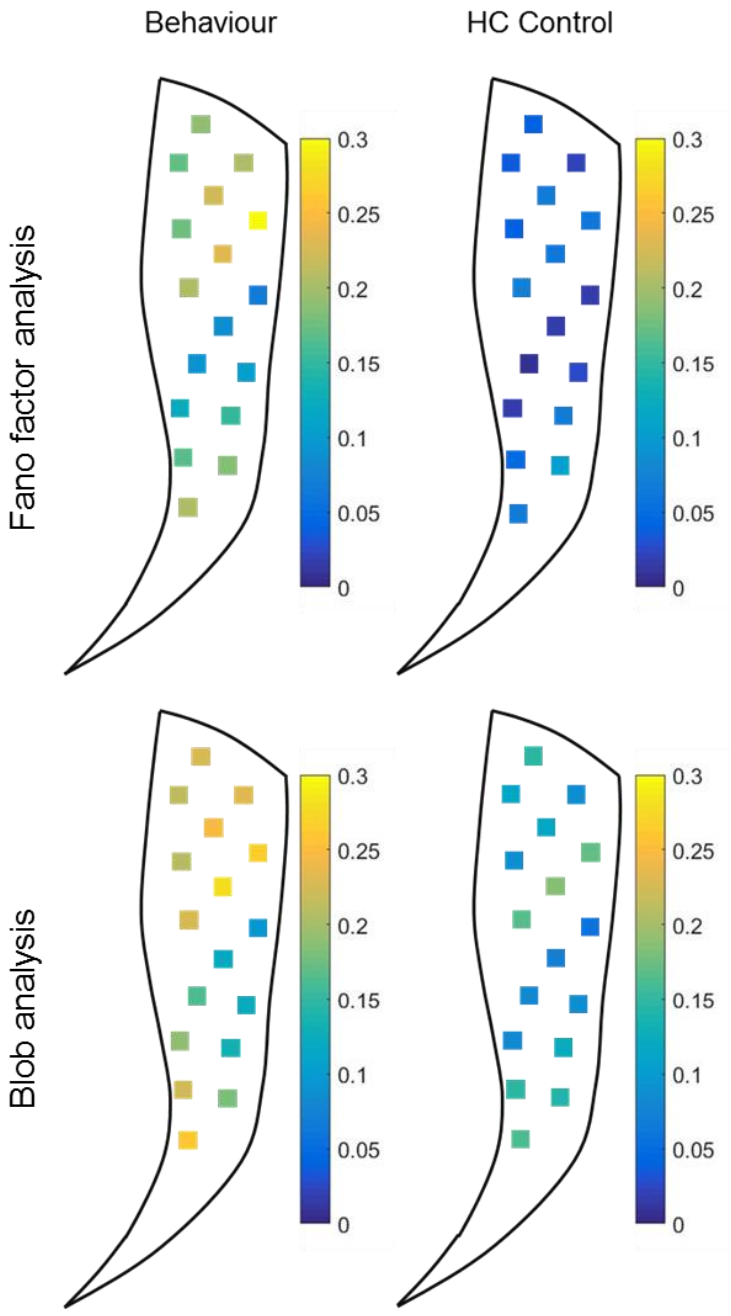

Figure 3.3. Proportion of IEG+ nuclei by sampled position on CA1 flatmap. Top: Fano factor analysis. IEG+ nuclei were defined as those having a fano factor value of 2 standard deviations above the home cage mean. Bottom: Blobs analysis. IEG+ nuclei were defined as those containing one or more blobs as detected with an automated analysis program (IEG_Analysis, see methods). Colourbar ranges from 0 (0%, dark blue) to 0.3 (30%, bright yellow).

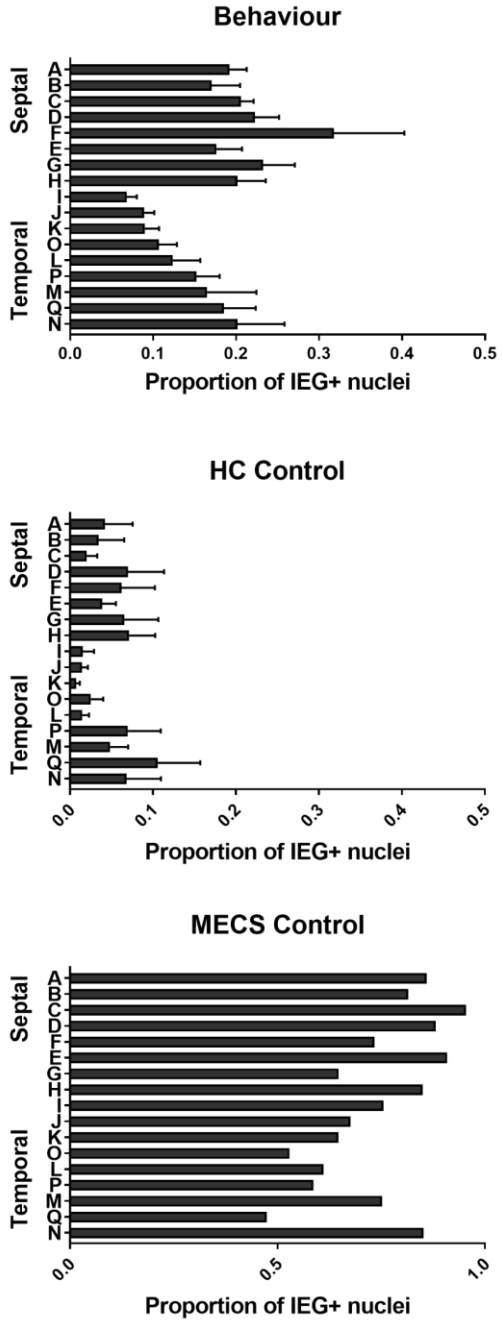

Figure 3.4. Proportion of IEG+ nuclei by relative position on the CA1 septotemporal axis. IEG+ neurons were defined as those having a fano factor value of 2 standard deviations above the home cage mean. Proportion of IEG+ nuclei by position from septal to temporal CA1 in behaviour (top), HC control (middle), and MECS control (bottom) conditions. Statistical comparisons (one-way ANOVAs) revealed a significant difference between positions in the behavior condition ($p<0.0019$), but not in the HC control condition. Labels (A-Q) correspond to position on CA1 flatmap. Error bars represent SEM.

Differences in IEG expression are not due to intrinsic differences in IEG expression between septotemporal regions

In order to ensure the IEG expression differences along the septotemporal axis were reflecting physiology and not just intrinsic gradients in the ability to express the IEG, maximal electroconvulsive shock (MECS) was used to induce gene expression in a positive control animal. Blob analysis was used to determine the proportion of IEG positive nuclei along the septotemporal axis, as was done with the behavioural and home cage control animals, except that the IEG used for MECS analysis was *Arc* (an IEG that is co-regulated with *Homer1a* (Vazdarjanova et. al., 2002)) (figure 3.5).

We used the proportion of IEG positive nuclei from the positive MECS control as a denominator for the proportions of IEG positive nuclei in the behavioural and home cage conditions. This was done so that the results reflect the proportion of nuclei that express these IEGs from the behavioural task out of the proportion of the population that are able to express these IEGs (figure 3.5). We found that this measure did not affect the overall pattern of IEG expression seen in figure 3.3.

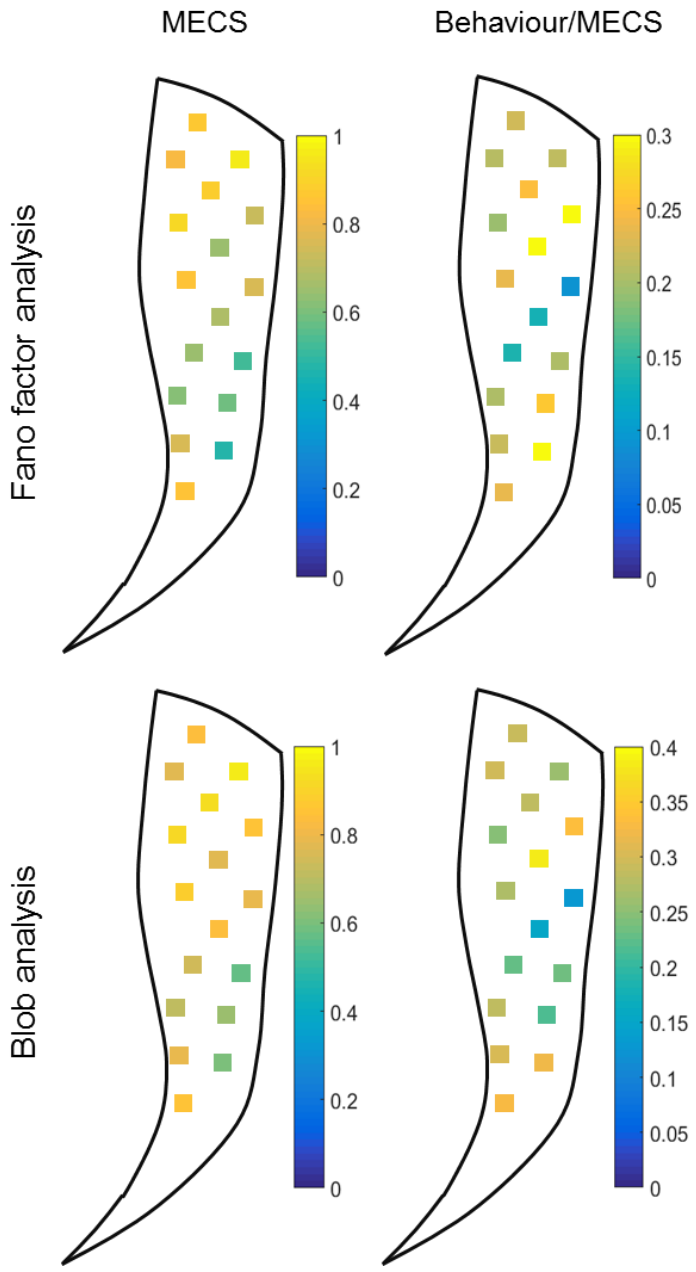

Figure 3.5. Characterization of the population of nuclei expressing IEGs following MECS induction. Left: MECS induced expression. Right: Behavioural data as a proportion of average IEG+ nuclei following MECS. Top: Fano factor analysis. Bottom: Blob analysis.

Normalized distributions of fano factor values reveal differences in the quantity of expression between septal, intermediate, and temporal CA1

Using fano factor values based on red pixel distribution within nuclei enabled the quantification of IEG expression in all nuclei, not just those characterized as IEG+. Using this method, we were able to characterize nuclei expressing even small amounts of IEGs, which enabled the detection of differences in the populations of neurons being examined.

Distribution comparisons of fano factor values between the behavioural and home cage control groups revealed differences in the two populations, as mentioned above (figure 3.1). Two-sample Kolmogorov-Smirnov tests also revealed significant differences in the distributions when comparing the behavioural and control groups in septal ($p<0.0001$), intermediate ($p<0.0001$), and temporal areas ($p<0.0001$) (figure 3.6).

Within group comparisons for differences in fano factor distributions between septal, intermediate, and temporal areas were also present. In the behavioural condition, there was a significant difference between septal and temporal areas, and intermediate and temporal areas ($p<0.0001$ for both, with a post hoc Bonferroni alpha value of 0.017 for multiple comparisons), but no statistical difference between septal and intermediate areas ($p=0.1302$). Statistical tests also revealed a significant difference between septal and temporal distributions in the home cage control animals ($p=0.0030$, also with a post hoc Bonferroni alpha value of 0.017 for multiple comparisons), but not between septal and intermediate ($p=0.7138$) or intermediate and temporal (0.2253).

Sparsity values calculated based on fano factor distributions were higher in septal CA1 as compared to temporal CA1 in behavior, but not in the home cage control. Sparsity values are presented in figure 3.6.

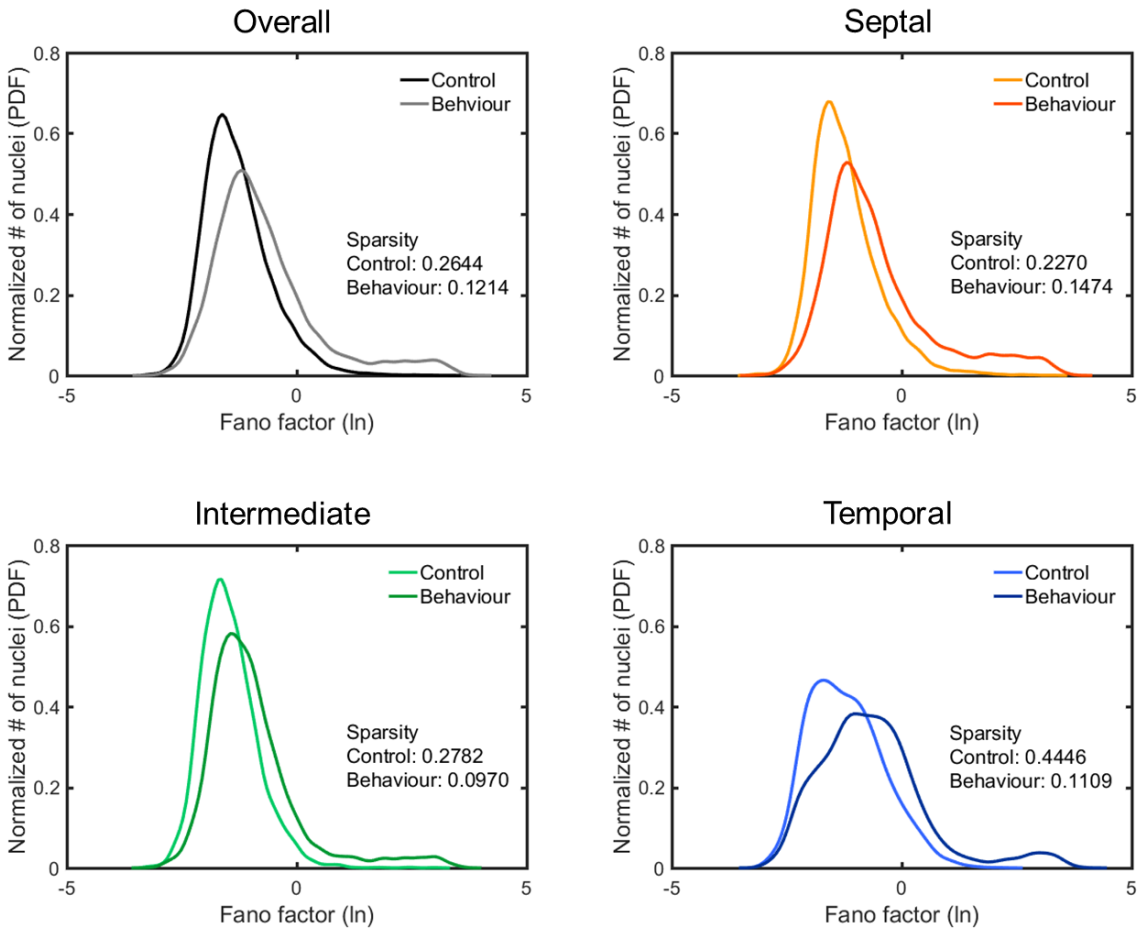

Figure 3.6. Normalized distributions of fano factor values and in behaviour and home cage control groups and corresponding sparsity values. Top: Normalized distributions of all nuclei comparing behaviour and control groups (p<0.0001). Bottom: Normalized distributions of nuclei comparing behaviour and control groups in (l-r): septal (p<0.0001), intermediate (p<0.0001), and temporal(p<0.0001) CA1 areas.

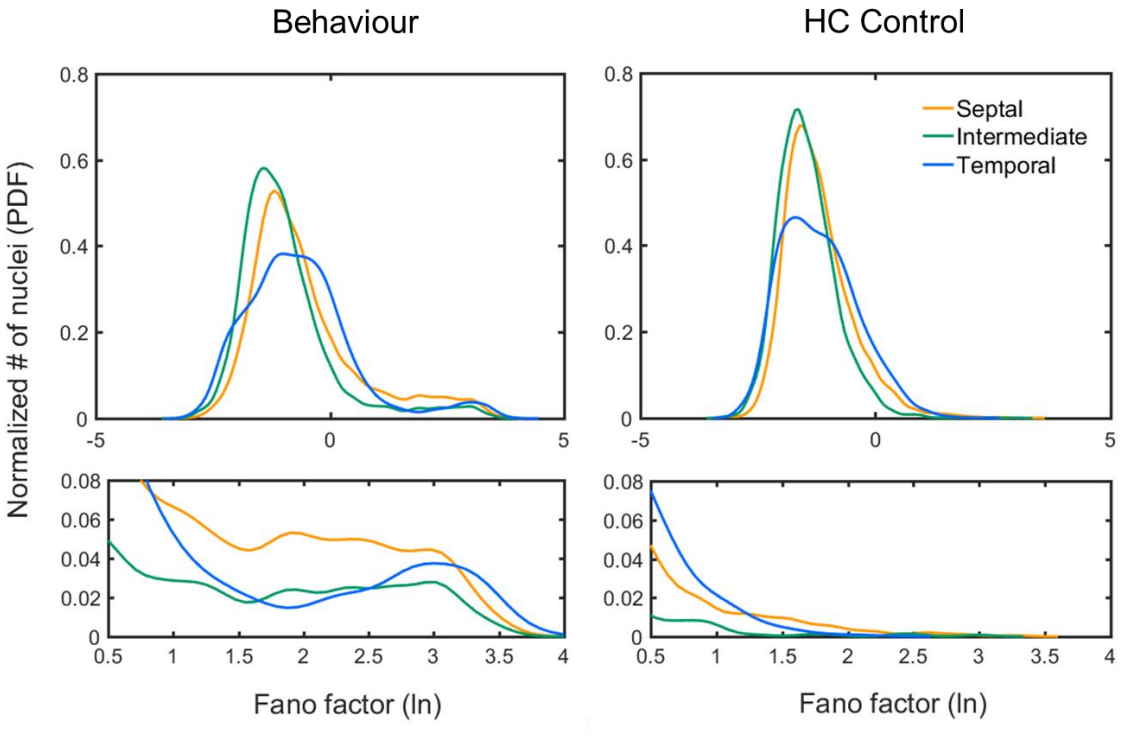

Figure 3.7. Normalized distributions of fano factor values in septal, intermediate, and temporal CA1. Graph on the top represents data for all nuclei, bottom figure is zoomed in on the right tail of the top figure. Left: Behavioural group. Right: Home cage control group.

Characterization of nuclei by number of blobs

In order to ensure the increase in expression seen in temporal CA1 could not be accounted for by an increase in cells expressing single blobs (which could potentially be an indication of less spiking activity), rather than the two blobs per nucleus that would be expected given the bi-allelic expression patterns normally described for *Homer1a*, we characterized the number of blobs per nuclei for septal, intermediate, and temporal CA1. We found that the proportion of nuclei that had zero, one, or two blobs was on average was 74.1%, 14.1%, and 11.8% for the behavioural group, and 88.8%, 8.6%, and 2.6% for home cage control animals, but these values varied depending on the septotemporal position (figure 3.7). The ratio of single blobs nuclei to double blobs nuclei for septal, intermediate, and temporal areas, respectively, were 1.2, 1.4, and 1.0 (behavioural group) and 3.3, 5.2, and 2.6 (control group). The normalized distributions for fano factor values in nuclei with two blobs revealed differences in the shape of the distributions of fano values, indicating that having a second blobs in the nucleus usually increases the fano factor value (figure 3.8 and figure 3.9).

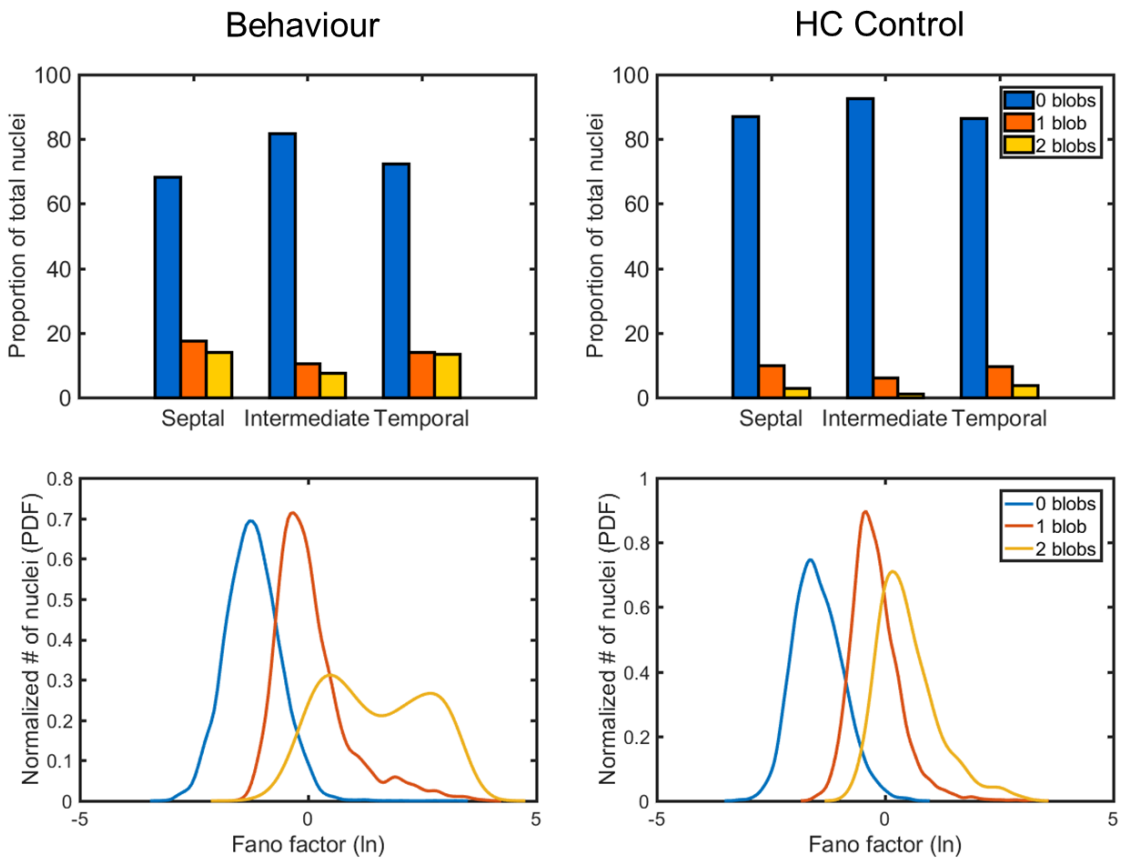

Figure 3.8. Characterization of nuclei by number of blobs. Top: Proportion of nuclei containing zero, one, and two blobs per nuclei in septal, intermediate, and temporal CA1. Bottom: The normalized fano factor distributions of nuclei containing zero, one, and two blobs. Left: Behavioural group. Right: Home cage control group.

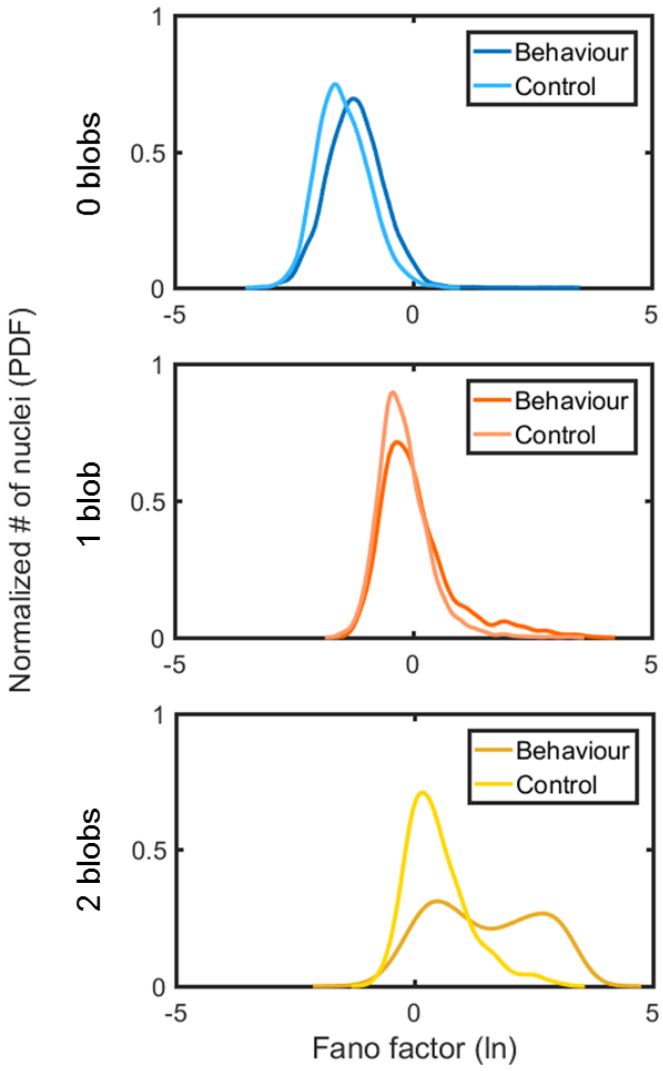

Figure 3.9. Normalized distributions of fano factor values based on the number of blobs. Distributions for behavior and home cage control nuclei with zero (top), one (middle), or two (bottom) blobs per nucleus.

CHAPTER 4: DISCUSSION

We mapped behaviourally-induced IEG transcriptional activity of neurons throughout the longitudinal axis of CA1 following the exploration of a novel environment. Using automated nuclear segmentation and IEG quantification methods, we were able to calculate not only the proportion of transcriptionally active neurons along the septotemporal axis, but also to characterize IEG expression in the entire population of neurons from experimental and control animals. We mapped ROIs from coronal sections onto a 2 dimensional hippocampal flat map in order to visualize the activity of neurons throughout CA1 in both the septotemporal and proximodistal axis. Contrary to predictions from either neurophysiology, connectivity or patterns of expression of other genes, our results indicate that there are two distinct domains along the septotemporal axis of CA1.

Proportion of IEG+ neurons did not follow the predicted pattern along the septotemporal axis of CA1

Our results do not align with what was predicted from current physiological data. We expected a gradient along the axis, with a greater proportion of cells active in septal CA1 as compared to temporal CA1. Instead, we found what seems to be a functional domain in septal CA1 and a functional gradient through intermediate and temporal CA1. We have termed these domains CA1d1 (septal) and CA1d2 (temporal) (figure 4.1). These domains correspond to roughly the septal half of and the temporal half of CA1, respectively.

These results could be due to a number of possibilities. Current data on the physiology of CA1 along the septotemporal axis is restricted to septal and intermediate regions (Jung et. al., 1994; Maurer et. al., 2005), and our predictions were based on a continuation of this trend throughout the septotemporal axis. This assumption of continuity was influenced by data showing that the trend of place field size expansion seen in septal to intermediate CA1 was the case for CA3 along the entire septotemporal axis (Kjelstrup et. al. 2008) (at least in terms of the size of place fields along the septotemporal axis, as the proportion of neurons active along the axis was not described in that study).

While our results could indicate that neurons in temporal regions of CA1 do not show the same pattern of activity as described in septal to intermediate CA1 and temporal CA3, they could also indicate that some proportion of neurons in temporal CA1 are not spatially modulated, which would make it difficult to detect using standard electrophysiological methods and experimental setups designed to investigate spatial processing in the brain. However, further experiments will need to be done to explore the implications of these findings. Some possible experiments will be detailed in the future research section of this chapter.

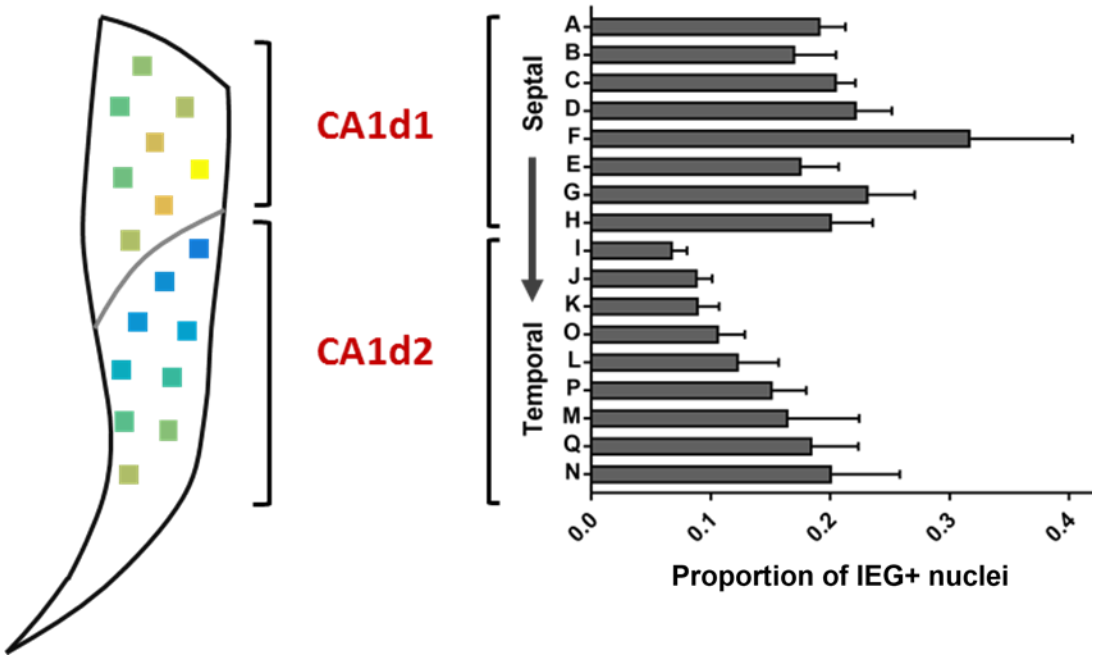

Figure 4.1 Proportion of IEG+ nuclei along the sepotemporal axis correspond to two domains. Hippocampal flat map representation and graphic representation of differences in IEG+ nuclei along the septotemporal axis.

Delineation in direct amygdalar input to CA1 approximately corresponds to proposed distinction between CA1d1 and CA1d2 domains

CA1 and other areas of the hippocampal formation have direct reciprocal connections with the amygdala. It has been demonstrated that direct amygdalar inputs to CA1 are mainly localized to the temporal half of CA1 (Petrovich, Canteras, & Swanson, 2001). These inputs have been shown to modulate neural activity in CA1 (Vouimba & Richter-Levin, 2005; Gosh et. al., 2013). This, along with lesion studies, has contributed to the hypothesis that temporal areas of the hippocampus are involved mostly in emotional or affective aspects of memory.

Indeed, when flatmap images of amygdalar input to the hippocampus are overlaid with CA1 flatmap images of data presented here on the proportion of IEG+ nuclei, there is a striking similarity between the approximate borders of amygdalar input (especially for certain nuclei like posterior area of the basolateral nucleus (BLAp), but also generally for total amygdalar input), and the domains for the septotemporal axis of CA1 proposed here. Data on the proportion of IEG+ nuclei in CA1 (from figure 3.5) from this thesis overlaid onto hippocampal flatmaps from Petrovich, Canteras, & Swanson (2001) are shown in figure 4.2. Interestingly, temporal CA3 does not show the same degree of skewed septotemporal distribution of amygdalar inputs.

Variation in inhibition along the septotemporal axis

The results presented here, specifically the sudden decrease in the proportion of IEG+ nuclei at the delineation of CA1d1 and CA1d2, could also indicate that there are differences in the distribution of inhibition along the septotemporal axis. It has been

demonstrated in slice preparations that cells in temporal CA1 are intrinsically more excitable than cells in septal CA1 (Dougherty et. al., 2012; Hönigsperger et. al., 2015; Malik et. al., 2015; Milior et. al., 2016), and that this is due to differences in inhibition between septal and temporal areas (Petrides et. al. 2007). However, how gradually or abruptly this inhibition changes along the axis has not been well characterized.

It is also known that there exists a diverse population of interneurons in the hippocampus (Soltesz, 2005), and that the targets of some of these types of interneurons non-uniformly inhibit specific laminar and functional subpopulations of hippocampal cells (Lee, et. al., 2014). Given this, it could be the case that the precise distribution of inhibitory inputs from different types of hippocampal interneurons demonstrate position-based bias along the septotemporal axis. It is possible that differences in the type and extent of inhibition could influence the expression of immediate early genes to produce what appears to be two domains, as presented in figure 4.1.

Total synaptic input vs. spiking

Another way in which variation in inhibition along the septotemporal axis could impact these results is that IEG expression could be regulated less by spiking per se, and more by total synaptic input. Depending on the specific relationship between excitation and inhibition along the axis, and its influence on spiking activity versus regional and total excitatory synaptic input, it could be the case that synaptic input is sufficient to trigger the initiation of molecular signaling cascades that induce the transcription of certain IEGs, even in cells that do not reach threshold for an action potential.

Because *Homer1a* transcription is modulated by the transcription factor CREB, this would require the activation of CREB (through phosphorylation of its active site) without producing an action potential. Indeed, it has been shown that calcium influx at even distal dendrites has a global effect on neurons, through mechanisms like the transport of calcium regulated proteins from the synapse to the nucleus (ex. Deisseroth et. al., 1998; Hagenston & Bading, 2011), although studies suggest that at minimum dendritic action potentials are needed for nuclear calcium dependent proteins, like CPB (CREB binding protein), to be activated (Hardingham et. al., 2001; Bading, 2013). Still, this decoupling between spiking activity and IEG expression could result in the difference between the results presented here and electrophysiological studies.

Left vs. right hemispheres

In the current study, IEG expression was only analyzed in the left hemisphere of the brain of each animal. There are, however, differences in the molecular, morphological and functional characteristics between the left and right hemispheres, such as the asymmetrical expression of NMDA receptor subunit NR2B (Kawakami et. al., 2003; Shinohara et. al., 2008; Shipton et. al., 2014). These differences could potentially influence the expression of IEGs; therefore, comparisons of IEG expression along the septotemporal axis between the left and right hemispheres will be completed in future analyses.

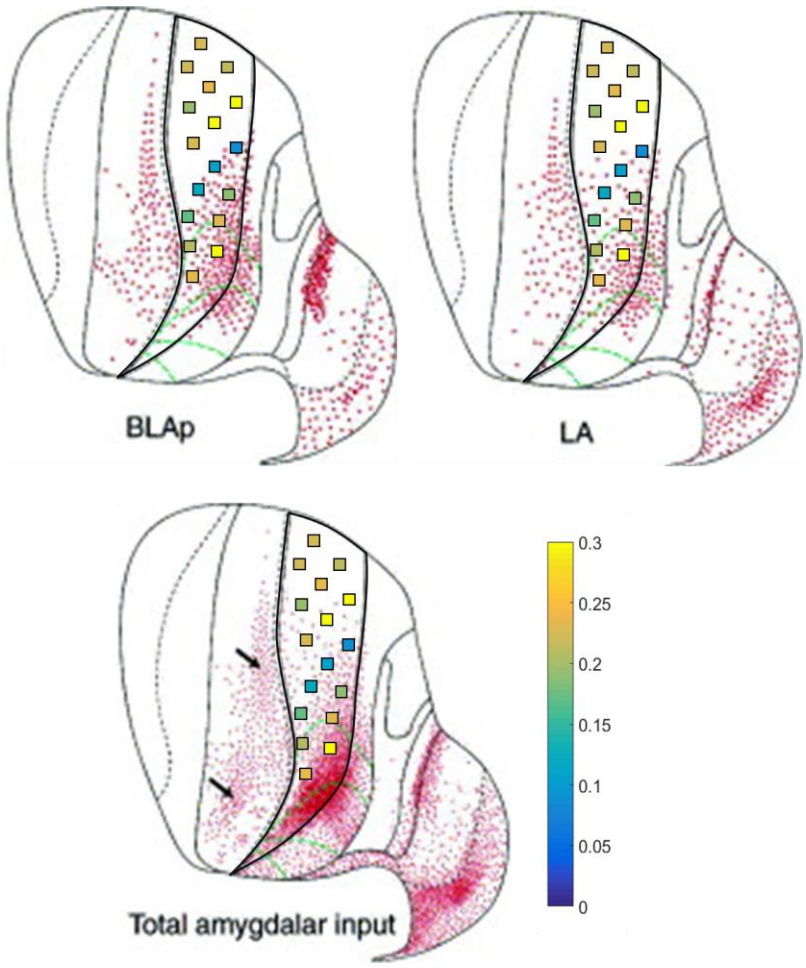

Figure 4.2 Overlay of physiological data from CA1 with amygdalar projections to the hippocampal formation on the hippocampal flat map. Results from the proportion of IEG+ nuclei (as measured with fano factor, and as a proportion of IEG+ nuclei from MECS) (figure 3.5) overlaid with data from amygdalar input from the posterior area of the basolateral nucleus (BLAp, top left), the lateral nucleus (LA, top right), and the total combined input from the amygdala from all nuclei examined (bottom). Colourbar indicates relative colours for the proportion of IEG+ nuclei. Flat maps modified from Petrovich, Canteras, & Swanson, 2001.

Distributions of IEG expression in all nuclei

Another goal of this project was to look at the quantification of IEG expressed throughout the entire population of neurons in behavioural and control groups. To do this, we measured the red variation within the nucleus using fano factor to enable the quantification of dispersed mRNA as well as blobs in all nuclei. This allowed the quantification of small amounts of IEG expression in all nuclei as it required no threshold, as opposed to only quantifying IEG blobs. In those nuclei that did contain blobs, fano factor was highly correlated with the integrated intensity of blobs, especially the largest blob in the nucleus in those that contained more than one (supplementary figure 5.8).

As predicted, the sparsity values calculated based on fano factor distributions were higher in septal CA1 as compared to temporal CA1 in behaviour (figure 3.6). This indicates that, while septal CA1 has a greater proportion of transcriptionally active cells, neurons in temporal CA1 express a greater quantity of IEG. However, sparsity values for intermediate CA1 were lower than those of temporal CA1. The unexpected increase in the proportion of IEG+ nuclei along the gradient in CA1d2 could explain this finding, although the precise relationship along the axis remains to be determined.

We found that the entire distribution of fano factor values in the behavioural group was right-shifted as compared to the home cage control distributions (figure 3.1). This indicates that there was some level of IEG expression in the majority of the neuronal

population in the behavioural group. Even in those nuclei that contained no blobs, the difference in the distribution can be seen between behavior and home cage control groups (figure 3.9).

This result could be due to a number of reasons. One suggestion is that the population of neurons active is higher than what is able to be resolved from current electrophysiological studies, with cells that fire only a small amount not being recognized with available analysis methods. Another suggestion, detailed above, is that synaptic input may be enough to trigger some amount of IEG expression in the nucleus, so that even cells that do not reach threshold for an action potential express some amount of *Homer1a*.

Nuclei with 1 vs. 2 blobs

One observation made previously (Demchuk, 2013; Demecha, 2013) in our lab that lines up with the results here is that many (more than half) nuclei that contain blobs only contain one blob, while normally two blobs are expected due to bi-allelic expression pattern normally seen for *Homer1a*. At first, it seemed possible that perhaps both alleles were being transcribed at the same transcription factory, and therefore appear as only one blob. In this case, we would expect that in nuclei containing one blob, the blob would have a higher integrated intensity than blobs in nuclei containing two blobs. However, in these results the average integrated intensity of blobs in single blob nuclei was lower than that of the average of the two blobs in double blob nuclei. Another related observation when examining fano factor values between the behaivoural and home cage control groups is that nuclei with only one blob had a more similar fano factor distribution

between groups than those that had zero or two blobs. Whether this finding is of significance for IEG quantification is not known.

Future research

The CA1 septotemporal axis

While there seems to be a relationship between the domains of CA1 proposed here and direct amygdalar input, a causal relationship has not been described. In order to examine whether the difference in patterns of neuronal activation between CA1d1 and CA1d2, and the gradient seen within CA1d2, are influenced by amygdalar input (and whether different nuclei within the amygdala affect the IEG expression differentially), additional experiments will have to be completed.

The most obvious experiment to test causality would be to disrupt input from the amygdala to the hippocampus. This could be done reversibly through the infusion of lidocaine or muscimol into the amygdala. Alternatively, the use of genetic technologies could enable the inactivation of only those neurons in the amygdala that specifically project to CA1, through the combined use of anterograde tracer Cre conjugates and optogenetics or DREADDs.

Another experiment that could prove useful in explaining the data at hand would be to use a dual IEG paradigm in which an animal is exposed to a neutral room for the induction of one gene (ex. *Homer1a*), and then is exposed to the same room again for the induction of another gene (ex. *Arc*), but with sounds or smells that would induce a fear response (such as a foot shock or cat smell). This experimental setup would aim to reduce

differences in neural activity caused by differences in space, but enhance differences in activity caused the affect of the animal.

Finally, future analysis of this work will include characterizing IEG expression along the septotemporal axis of CA3, since the physiology of CA3 along the more temporal regions of the axis has been more extensively characterized. This will allow a more direct comparison of IEG data with physiological data.

REFERENCES

Al-Kofahi, Y., Lassoued, W., Lee, W., & Roysam, B. (2010). Improved automatic detection and segmentation of cell nuclei in histopathology images. *IEEE Transactions on Biomedical Engineering*, *57*(4), 841-852.

Amaral, D. G., & Witter, M. P. (1989). The three-dimensional organization of the hippocampal formation: a review of anatomical data. *Neuroscience*, *31(3)*, 571-591.

Andersen, P., Bliss, T. V. P., & Skrede, K. K. (1971). Lamellar organization of hippocampal excitatory pathways. *Experimental Brain Research*, *13*(2), 222-238.

Andersen, P., Holmqvist, B., & Voorhoeve, P. E. (1966). Entorhinal activation of dentate granule cells. *Acta physiologica Scandinavica*, *66*(4), 448-460.

Bading, H. (2013). Nuclear calcium signalling in the regulation of brain function. *Nature Reviews Neuroscience*, *14*(9), 593-608.

Bast, T., Wilson, I. A., Witter, M. P., & Morris, R. G. (2009). From rapid place learning to behavioral performance: a key role for the intermediate hippocampus. *PLoS Biol*, *7*(4), e1000089.

Bjornsson, C. S., Lin, G., Al-Kofahi, Y., Narayanaswamy, A., Smith, K. L., Shain, W., & Roysam, B. (2008). Associative image analysis: a method for automated quantification of 3D multi-parameter images of brain tissue. *Journal of neuroscience methods*, *170*(1), 165-178.

Bottai, D., Guzowski, J. F., Schwarz, M. K., Kang, S. H., Xiao, B., Lanahan, A., Worley P. F., & Seeburg, P. H. (2002). Synaptic activity-induced conversion of intronic to exonic sequence in Homer 1 immediate early gene expression. *The Journal of neuroscience*, *22*(1), 167-175.

Cembrowski, M. S., Bachman, J. L., Wang, L., Sugino, K., Shields, B. C., & Spruston, N. (2016). Spatial gene-expression gradients underlie prominent heterogeneity of CA1 pyramidal neurons. *Neuron*, *89*(2), 351-368.

Chawla, M.K., Lin, G., Olson, K., Vazdarjanova, A., Burke, S.N., McNaughton, B.L., Worley, P.F., Guzowski, J.F., Roysam, B., & Barnes, C.A. (2004). 3D-CatFISH: a system for automated quantitative three-dimensional compartmental analysis of temporal gene transcription activity imaged by fluorescence in situ hybridization. *Journal of Neuroscience Methods*, 139, 13-24.

Crepaldi, L., Policarpi, C., Coatti, A., Sherlock, W. T., Jongbloets, B. C., Down, T. A., & Riccio, A. (2013). Binding of TFIIIC to sine elements controls the relocation of

activity-dependent neuronal genes to transcription factories. *PLoS Genet, 9*(8), e1003699.

Deisseroth, K., Heist, E. K., & Tsien, R. W. (1998). Translocation of calmodulin to the nucleus supports CREB phosphorylation in hippocampal neurons. *Nature, 392*(6672), 198-202.

Demchuk, A. M. (2014). Non-uniform excitability of hippocampal neurons affords weak predictability of future immediate-early gene expression patterns (Master's thesis). University of Lethbridge, Alberta, Canada.

Demecha, A. (2013). Analysis of immediate early genes Arc and Homer1a detection methods in hippocampal remapping studies (Honours thesis). University of Lethbridge, Alberta, Canada.

Dolorfo, C. L., & Amaral, D. G. (1998). Entorhinal cortex of the rat: topographic organization of the cells of origin of the perforant path projection to the dentate gyrus. *Journal of Comparative Neurology, 398*(1), 25-48.

Dong, H. W., Swanson, L. W., Chen, L., Fanselow, M. S., & Toga, A. W. (2009). Genomic–anatomic evidence for distinct functional domains in hippocampal field CA1. *Proceedings of the National Academy of Sciences, 106*(28), 11794-11799.

Dougherty, K. A., Islam, T., & Johnston, D. (2012). Intrinsic excitability of CA1 pyramidal neurones from the rat dorsal and ventral hippocampus. *The Journal of physiology*, *590*(22), 5707-5722.

Du, G., Drexler, G. A., Friedland, W., Greubel, C., Hable, V., Krücken, R., Kugler, A., Tonelli, L., Friedl, A.A. & Dollinger, G. (2011). Spatial dynamics of DNA damage response protein foci along the ion trajectory of high-LET particles. *Radiation research*, *176*(6), 706-715.

Fanselow, M. S., & Dong, H. W. (2010). Are the dorsal and ventral hippocampus functionally distinct structures? *Neuron, 65(1),* 7-19.

Ghosh, S., Laxmi, T. R., & Chattarji, S. (2013). Functional connectivity from the amygdala to the hippocampus grows stronger after stress. *The Journal of Neuroscience, 33*(17), 7234-7244.

Guzowski, J.F. (2002). Insights into immediate-early gene function in hippocampal memory consolidation using antisense oligonucleotide and fluorescent imaging approaches. Hippocampus, 12, 86-104.

Guzowski, J. F., McNaughton, B. L., Barnes, C. A., & Worley, P. F. (1999). Environment-specific expression of the immediate-early gene Arc in hippocampal neuronal ensembles. *Nature neuroscience, 2*(12), 1120-1124.

Guzowski, J.F., Timlin, J.A., Roysam, B., McNaughton, B.L., Worley, P.F., & Barnes, C.A. (2005). Mapping behaviorally relevant neural circuits with immediate-early gene expression. *Current Opinion in Neurobiology*, *15*, 599-606.

Hafting, T., Fyhn, M., Molden, S., Moser, M. B., & Moser, E. I. (2005). Microstructure of a spatial map in the entorhinal cortex. *Nature*, *436*(7052), 801-806.

Hagenston, A. M., & Bading, H. (2011). Calcium signaling in synapse-to-nucleus communication. *Cold Spring Harbor perspectives in biology*, *3*(11), a004564.

Hardingham, G. E., Arnold, F. J., & Bading, H. (2001). Nuclear calcium signaling controls CREB-mediated gene expression triggered by synaptic activity. *Nature neuroscience*, *4*(3), 261-267.

Hönigsperger, C., Marosi, M., Murphy, R., & Storm, J. F. (2015). Dorsoventral differences in Kv7/M ‐ current and its impact on resonance, temporal summation and excitability in rat hippocampal pyramidal cells. *The Journal of physiology*, *593*(7), 1551-1580.

Hu, J. H., Park, J. M., Park, S., Xiao, B., Dehoff, M. H., Kim, S., Hayashi T., Schwarz M. K., Huganir R. L., Seeburg P. H., & Linden, D. J. (2010). Homeostatic scaling requires group I mGluR activation mediated by Homer1a. *Neuron*, *68*(6), 1128-1142.

Hunsaker, M. R., & Kesner, R. P. (2008). Dissociations across the dorsal–ventral axis of CA3 and CA1 for encoding and retrieval of contextual and auditory-cued fear. *Neurobiology of learning and memory*, *89*(1), 61-69.

Iborra, F. J., Pombo, A., Jackson, D. A., & Cook, P. R. (1996). Active RNA polymerases are localized within discrete transcription “factories' in human nuclei. *Journal of cell science*, *109*(6), 1427-1436.

Imamura, N., Nonaka, A., Yamamoto, H., Matsuki, N., & Nomura, H. (2011). Experience-dependent Homer1a expression in excitatory and inhibitory neurons. *Neuroreport*, *22*(7), 353-357.

Jay, T. M., & Witter, M. P. (1991). Distribution of hippocampal CA1 and subicular efferents in the prefrontal cortex of the rat studied by means of anterograde transport of Phaseolus vulgaris ‐ leucoagglutinin. *Journal of Comparative Neurology*, *313*(4), 574-586.

Jones, B. F., & Witter, M. P. (2007). Cingulate cortex projections to the parahippocampal region and hippocampal formation in the rat. *Hippocampus*, *17*(10), 957-976.

Jung, M. W., Wiener, S. I., & McNaughton, B. L. (1994). Comparison of spatial firing characteristics of units in dorsal and ventral hippocampus of the rat. *The Journal of neuroscience*, *14*(12), 7347-7356.

Kammermeier, P. J., & Worley, P. F. (2007). Homer 1a uncouples metabotropic glutamate receptor 5 from postsynaptic effectors. *Proceedings of the National Academy of Sciences*, *104*(14), 6055-6060.

Kawakami, R., Shinohara, Y., Kato, Y., Sugiyama, H., Shigemoto, R., & Ito, I. (2003). Asymmetrical allocation of NMDA receptor ε2 subunits in hippocampal circuitry. *Science*, *300*(5621), 990-994.

Keinath, A. T., Wang, M. E., Wann, E. G., Yuan, R. K., Dudman, J. T., & Muzzio, I. A. (2014). Precise spatial coding is preserved along the longitudinal hippocampal axis. *Hippocampus*, *24*(12), 1533-1548.

Kjelstrup, K. B., Solstad, T., Brun, V. H., Hafting, T., Leutgeb, S., Witter, M. P., Moser, E.I. & Moser, M.B. (2008). Finite scale of spatial representation in the hippocampus. *Science, 321(5885),* 140-143.

Kjelstrup, K. G., Tuvnes, F. A., Steffenach, H. A., Murison, R., Moser, E. I., & Moser, M. B. (2002). Reduced fear expression after lesions of the ventral hippocampus. *Proceedings of the National Academy of Sciences*, *99*(16), 10825-10830.

Krettek, J. E., & Price, J. L. (1977). Projections from the amygdaloid complex to the cerebral cortex and thalamus in the rat and cat. *Journal of Comparative Neurology*, *172*(4), 687-722.

Lee, S. H., Marchionni, I., Bezaire, M., Varga, C., Danielson, N., Lovett-Barron, M., Losonczy, A., & Soltesz, I. (2014). Parvalbumin-positive basket cells differentiate among hippocampal pyramidal cells. *Neuron*, *82*(5), 1129-1144.

Lein, E. S., Hawrylycz, M. J., Ao, N., Ayres, M., Bensinger, A., Bernard, A., Boe, A.F., Boguski, M.S., Brockway, K.S., Byrnes, E.J. & Chen, L. (2007). Genome-wide atlas of gene expression in the adult mouse brain. *Nature*, *445*(7124), 168-176.

Malik, R., Dougherty, K. A., Parikh, K., Byrne, C., & Johnston, D. (2015). Mapping the electrophysiological and morphological properties of CA1 pyramidal neurons along the longitudinal hippocampal axis. *Hippocampus*.

Maurer, A. P., VanRhoads, S. R., Sutherland, G. R., Lipa, P., & McNaughton, B. L. (2005). Self-motion and the origin of differential spatial scaling along the septo-temporal axis of the hippocampus. *Hippocampus 15*(7), 841.

McNaughton, B. L., Barnes, C. A., Meltzer, J., & Sutherland, R. J. (1989). Hippocampal granule cells are necessary for normal spatial learning but not for spatially-selective pyramidal cell discharge. *Experimental Brain Research*, *76*(3), 485-496.

Milior, G., Di Castro, M. A., Pepe'Sciarria, L., Garofalo, S., Branchi, I., Ragozzino, D., Limatola, C., & Maggi, L. (2016). Electrophysiological Properties of CA1 Pyramidal Neurons along the Longitudinal Axis of the Mouse Hippocampus. *Scientific Reports*, *6*, 38242.

Milner, B., & Penfield, W. (1955). The effect of hippocampal lesions on recent memory. *Transactions of the American Neurological Association*, (80th Meeting), 42.

Mitchell, J. A., & Fraser, P. (2008). Transcription factories are nuclear subcompartments that remain in the absence of transcription. *Genes & development*, *22*(1), 20-25.

Miyashita, T., Kubik, S., Haghighi, N., Steward, O., & Guzowski, J. F. (2009). Rapid activation of plasticity-associated gene transcription in hippocampal neurons provides a mechanism for encoding of one-trial experience. *The Journal of Neuroscience*, *29*(4), 898-906.

Montes‐Rodríguez, C. J., Lapointe, V., Trivedi, V., Lu, Q., Demchuk, A. M., & McNaughton, B. L. (2013). Postnatal development of Homer1a in the rat hippocampus. *Hippocampus*, *23*(10), 890-902.

Moser, M. B., & Moser, E. I. (1998). Functional differentiation in the hippocampus. *Hippocampus*, *8(6)*, 608-619.

Moser, E., Moser, M. B., & Andersen, P. (1993). Spatial learning impairment parallels the magnitude of dorsal hippocampal lesions, but is hardly present following ventral lesions. *The Journal of Neuroscience*, *13*(9), 3916-3925.

Moser, M. B., Moser, E. I., Forrest, E., Andersen, P., & Morris, R. G. (1995). Spatial learning with a minislab in the dorsal hippocampus. *Proceedings of the National Academy of Sciences*, *92*(21), 9697-9701.

O'Keefe, J., & Dostrovsky, J. (1971). The hippocampus as a spatial map. Preliminary evidence from unit activity in the freely-moving rat. *Brain research*, *34*(1), 171-175.

O'Keefe, J., & Nadel, L. (1978). *The hippocampus as a cognitive map*. Oxford University Press, USA.

Parent, M. A., Wang, L., Su, J., Netoff, T., & Yuan, L. L. (2010). Identification of the hippocampal input to medial prefrontal cortex in vitro. *Cerebral Cortex*, *20*(2), 393-403.

Penner, M.R., Roth, T.L., Chawla, M.K., Hoang, L.T., Roth, E.D., Lubin, F.D., Barnes, C.A. (2011). Age-related changes in Arc transcription and DNA methylation within the hippocampus. Neurobiology of Aging, 32, 2198-2210.

Petrides, T., Georgopoulos, P., Kostopoulos, G., & Papatheodoropoulos, C. (2007). The GABAA receptor-mediated recurrent inhibition in ventral compared with dorsal CA1 hippocampal region is weaker, decays faster and lasts less. *Experimental brain research*, *177*(3), 370-383.

Petrovich, G. D., Canteras, N. S., & Swanson, L. W. (2001). Combinatorial amygdalar inputs to hippocampal domains and hypothalamic behavior systems. *Brain Research Reviews*, *38(1),* 247-289.

Saha, R. N., Wissink, E. M., Bailey, E. R., Zhao, M., Fargo, D. C., Hwang, J. Y., Daigle K. R., Fenn J. D., Adelman K., & Dudek, S. M. (2011). Rapid activity-induced transcription of Arc and other IEGs relies on poised RNA polymerase II. *Nature neuroscience*, *14*(7), 848-856.

Scoville, W. B. (1954). The Limbic Lobe in Man*. *Journal of neurosurgery*, *11*(1), 64-66.

Scoville, W. B., & Milner, B. (1957). Loss of recent memory after bilateral hippocampal lesions. *Journal of Neurology, Neurosurgery & Psychiatry*, *20*(1), 11-21.

Shinohara, Y., Hirase, H., Watanabe, M., Itakura, M., Takahashi, M., & Shigemoto, R. (2008). Left-right asymmetry of the hippocampal synapses with differential subunit allocation of glutamate receptors. *Proceedings of the National Academy of Sciences*, *105*(49), 19498-19503.

Shipton, O. A., El-Gaby, M., Apergis-Schoute, J., Deisseroth, K., Bannerman, D. M., Paulsen, O., & Kohl, M. M. (2014). Left–right dissociation of hippocampal memory processes in mice. *Proceedings of the National Academy of Sciences*, *111*(42), 15238-15243.

Shiraishi-Yamaguchi, Y., & Furuichi, T. (2007). The Homer family proteins. *Genome biology*, *8*(2), 1.

Soltesz, I. (2005). *Diversity in the neuronal machine: order and variability in interneuronal microcircuits*. Oxford University Press.

Stensola, H., Stensola, T., Solstad, T., Frøland, K., Moser, M. B., & Moser, E. I. (2012). The entorhinal grid map is discretized. *Nature*, *492*(7427), 72-78.

Strange, B. A., Witter, M. P., Lein, E. S., & Moser, E. I. (2014). Functional organization of the hippocampal longitudinal axis. *Nature Reviews Neuroscience, 15(10),* 655-669.

Sutherland, H., & Bickmore, W. A. (2009). Transcription factories: gene expression in unions?. *Nature Reviews Genetics, 10*(7), 457-466.

Sutherland, R. J., Whishaw, I. Q., & Kolb, B. (1983). A behavioural analysis of spatial localization following electrolytic, kainate-or colchicine-induced damage to the hippocampal formation in the rat. *Behavioural brain research, 7(2),* 133-153.

Sutherland, R. J., Sparks, F. T., & Lehmann, H. (2010). Hippocampus and retrograde amnesia in the rat model: a modest proposal for the situation of systems consolidation. *Neuropsychologia*, *48*(8), 2357-2369.

Swanson, L. W. (1981). A direct projection from Ammon's horn to prefrontal cortex in the rat. *Brain research*, *217*(1), 150-154.

Swanson, L. W., & Cowan, W. M. (1977). An autoradiographic study of the organization of the efferet connections of the hippocampal formation in the rat. *Journal of Comparative Neurology*, *172*(1), 49-84.

Swanson, L. W., Wyss, J. M., & Cowan, W. M. (1978). An autoradiographic study of the organization of intrahippocampal association pathways in the rat. *Journal of comparative neurology*, *181*(4), 681-715.

Takata, N., Yoshida, K., Komaki, Y., Xu, M., Sakai, Y., Hikishima, K., Mimura M., Okano H., & Tanaka, K. F. (2015). Optogenetic activation of CA1 pyramidal neurons at the dorsal and ventral hippocampus evokes distinct brain-wide responses revealed by mouse fMRI. *PLoS one, 10*(3), e0121417.

Terrazas, A., Krause, M., Lipa, P., Gothard, K. M., Barnes, C. A., & McNaughton, B. L. (2005). Self-motion and the hippocampal spatial metric. *The Journal of neuroscience*, *25*(35), 8085-8096.

Thompson, C. L., Pathak, S. D., Jeromin, A., Ng, L. L., MacPherson, C. R., Mortrud, M. T., Cusick, A., Riley, Z.L., Sunkin, S.M., Bernard, A. & Puchalski, R. B. (2008). Genomic anatomy of the hippocampus. *Neuron*, *60*(6), 1010-1021.

Tushev, G., & Schuman, E. M. (2016). Rethinking Functional Segregation: Gradients of Gene Expression in Area CA1. *Neuron*, *89*(2), 242-243.

Vago, D. R., & Kesner, R. P. (2008). Disruption of the direct perforant path input to the CA1 subregion of the dorsal hippocampus interferes with spatial working memory and novelty detection. *Behavioural brain research*, *189*(2), 273-283.

Vazdarjanova, A., McNaughton, B. L., Barnes, C. A., Worley, P. F., & Guzowski, J. F. (2002). Experience-dependent coincident expression of the effector immediate-early genes arc and Homer 1a in hippocampal and neocortical neuronal networks. *The Journal of neuroscience*, *22*(23), 10067-10071.

Vouimba, R. M., & Richter-Levin, G. (2005). Physiological dissociation in hippocampal subregions in response to amygdala stimulation. *Cerebral Cortex*, *15*(11), 1815-1821.

Wilber, A. A., Clark, B. J., Demecha, A. J., Mesina, L., Vos, J. M., & McNaughton, B. L. (2014). Cortical connectivity maps reveal anatomically distinct areas in the parietal cortex of the rat. *Frontiers in neural circuits*, *8*.

Witharana, W. K. L (2011). Non-boolean characterization of homer1a intranuclear transcription foci (Master's thesis). University of Lethbridge, Alberta, Canada.

Witharana, W. K. L., Cardiff, J., Chawla, M. K., Xie, J. Y., Alme, C., Eckert, M., Lapointe V., Demchuk A., Maurer A. P., Trivedi V., Sutherland R. J., Guzowski, J. F., Barnes, C. A., & McNaughton, B. L. (2016). Nonuniform allocation of hippocampal neurons to place fields across all hippocampal subfields. *Hippocampus*, *26*: 1328–1344.

Witharana, W.K.L., Clark, B.J., Trivedi, V., Lapointe, V., and McNaughton, B.L. (2012) Integrated fluorescence intensity of Homer1a transcription foci indicate integrated neuronal firing rates. *Society for Neuroscience Annual International Meeting: Neuroscience 2012* (Oct 12- 17), New Orleans, LA, USA. (Poster)

APPENDICIES

A. Supplementary Methods

Imaging

NanoZoomer

All slides were first imaged using a NanoZoomer (Hammamatsu) digital microscope. Slides were loaded (six at a time) into the machine on batch mode, and scan areas and focus points were applied manually. Focusing was done automatically. The following scanning parameters were used:

Profile – Fluorescence/brightfield
Exposure – 2x
Colour balance – red 3x, blue 3x, green 3x
Resolution – 40x.

Confocal

Following NanoZoomer imaging, each slide was imaged using a confocal microscope. All images were created usng 1024x1024 pixels per frame. The following scan parameters were used:

DAPI: Laser: 5.1% power
HV: 460-475HV gain
Texas Red: Laser: 5.0% power
HV: 520 - 570 gain.

Image Analysis

Blob detection thresholds

Table 5.1. Parameters and user settings for automated blob detection with IEG Analysis.

Parameter	**User settings**	**Description**
Minimum blue	30	Minimum blue threshold for background (nucleus)
Minimum blue percentage	40	Minimum percentage of blob background that muse contain the minimum blue threshold
Minimum peak red	50	Threshold for highest intensity pixels
Minimum red threshold	30	Minimum threshold for pixels to be included in blob
Minim red pixels	8	Minimum blob volume in pixels
Maximum red pixels	5200	Maximum blob volume in pixels
Minimum z-stacks	4	Minimum number of z-planes the blob must pass through

Total red analysis

In order to characterize the total red within nuclei, we summed the red value of each pixel within segmented nuclei. We then calculated the mean total red across nuclei and across animals within each ROI (figure 5.2, figure 5.3). In addition, we applied background subtraction, since the total red within each nucleus is affected by background red and variations in nuclear volume. The background value of each image was calculated by first expanding nuclear boundaries, then taking the average value of red in each pixel outside the expanded nuclear borders. This value was then subtracted from each pixel in the image. We then calculated the mean total red across nuclei and across animals within each ROI following background subtraction (figure 5.4, figure 5.5).

B. Supplementary Results

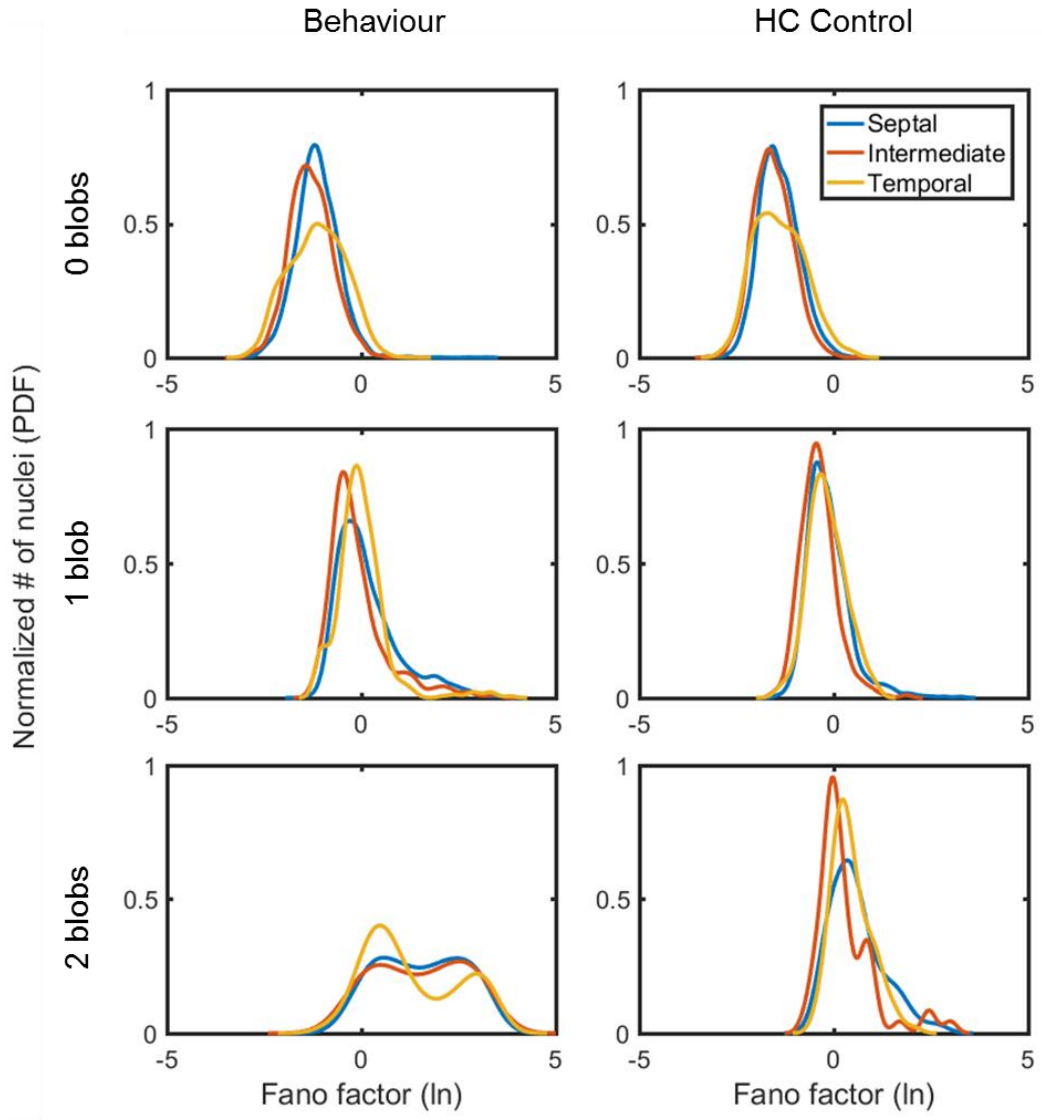

Figure 5.1 Normalized distributions of fano factor values based on blobs number in septal, intermediate, and temporal CA1.

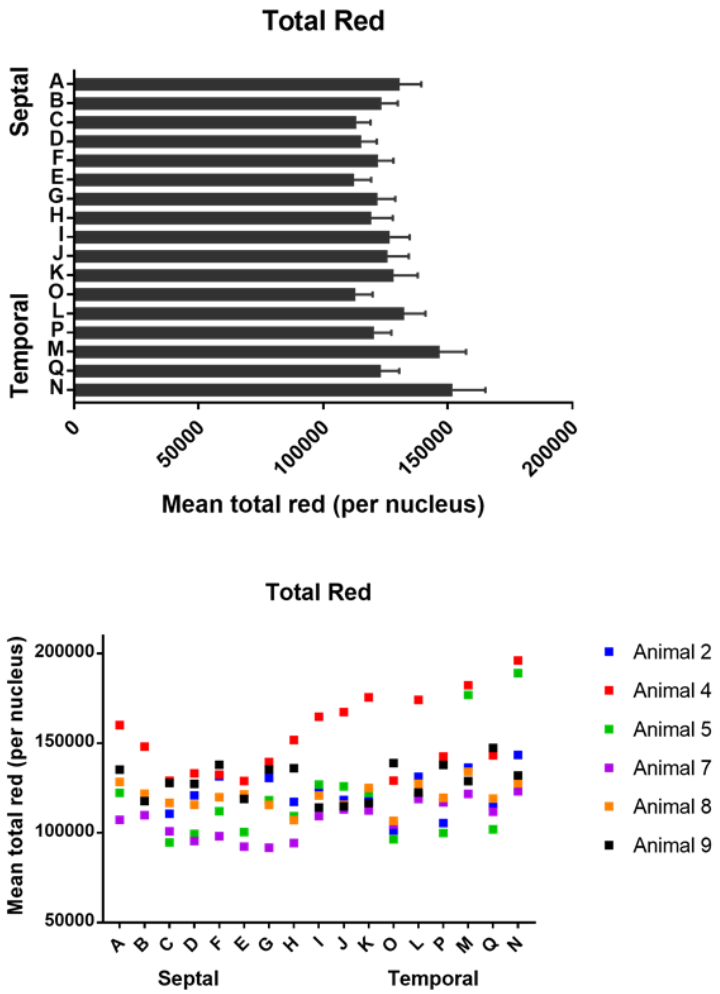

Figure 5.2. Mean total red values by relative position on CA1 septotemporal axis in behavioural condition. Top: Mean total red values per nucleus, averaged across animals. Error bars represent SEM. Bottom: Mean total red values per nucleus for each individual animal.

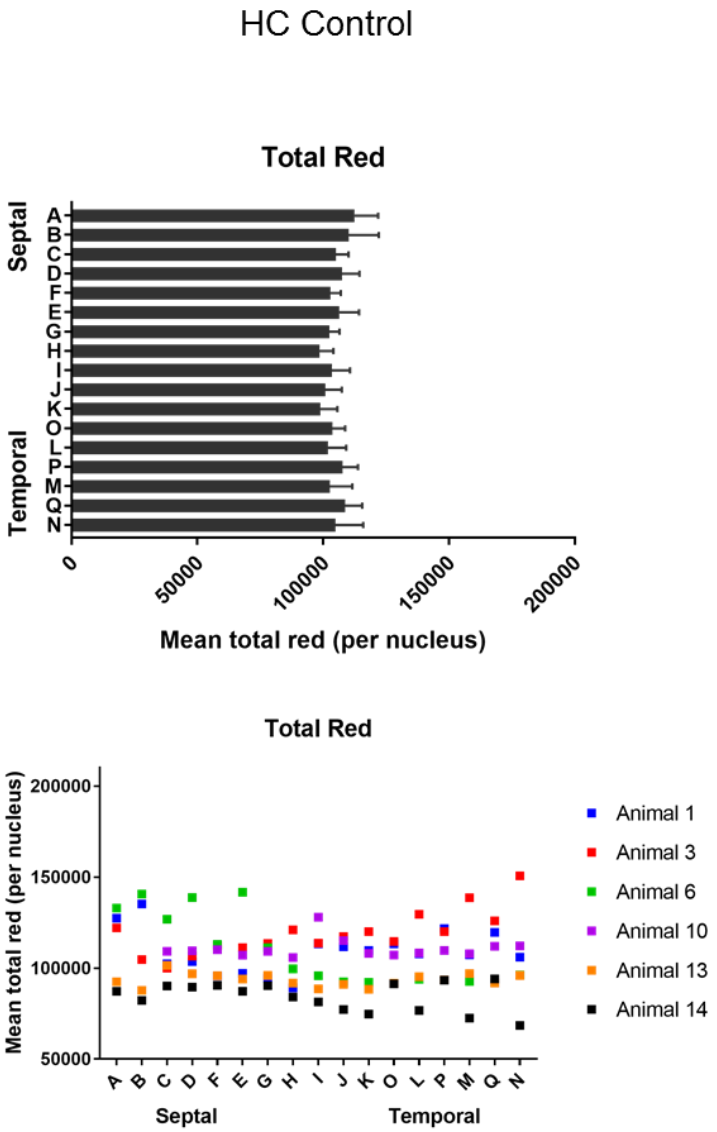

Figure 5.3. Mean total red values by relative position on CA1 septotemporal axis in home cage control condition. Top: Mean total red values per nucleus, averaged across animals. Error bars represent SEM. Bottom: Mean total red values per nucleus for each individual animal.

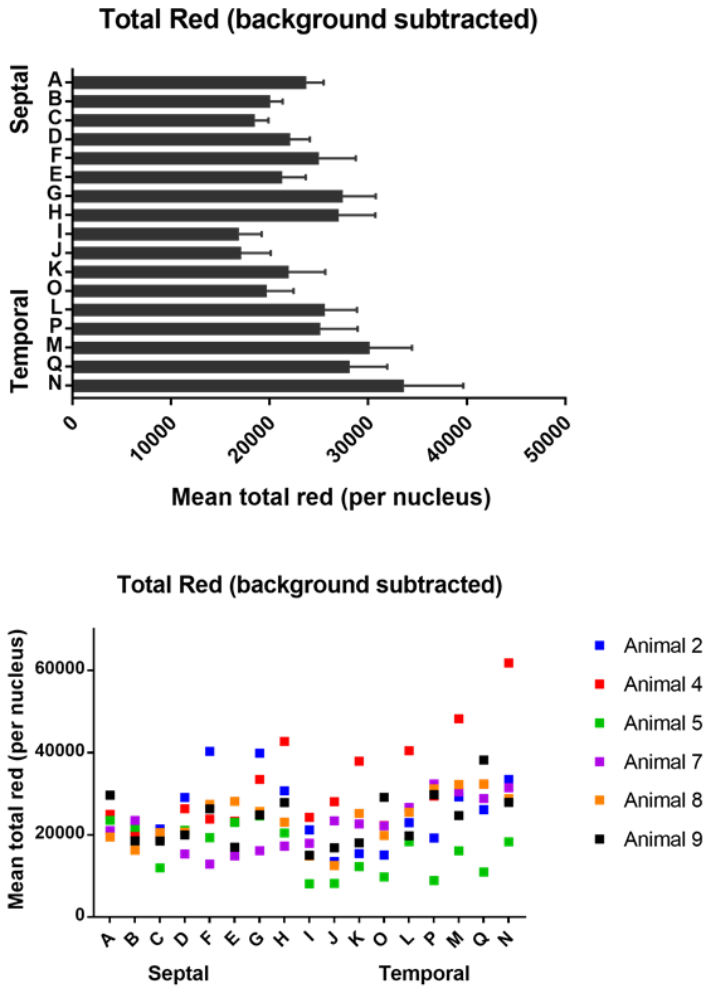

Figure 5.4. Mean total red values after background subtraction by relative position on CA1 septotemporal axis in behavioural condition. Top: Mean total red values per nucleus after background subtraction, averaged across animals. Error bars represent SEM. Bottom: Mean total red values per nucleus after background subtraction for each individual animal.

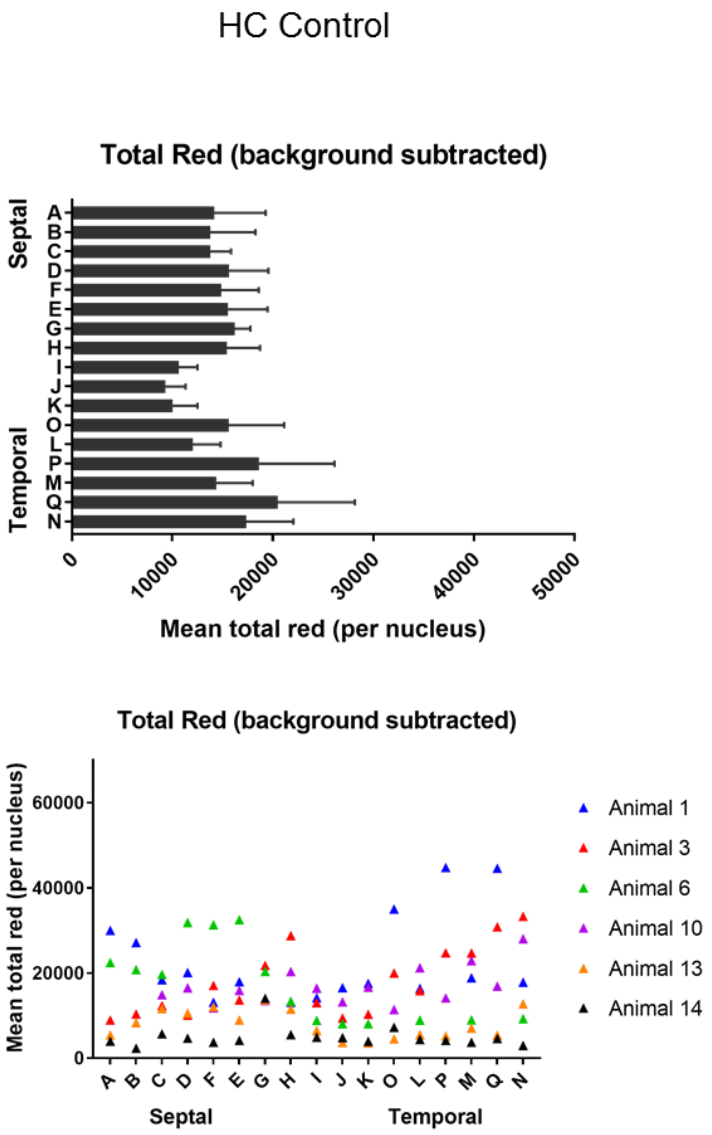

Figure 5.5. Mean total red values after background subtraction by relative position on CA1 septotemporal axis in HC control condition. Top: Mean total red values per nucleus after background subtraction, averaged across animals. Error bars represent SEM. Bottom: Mean total red values per nucleus after background subtraction for each individual animal.

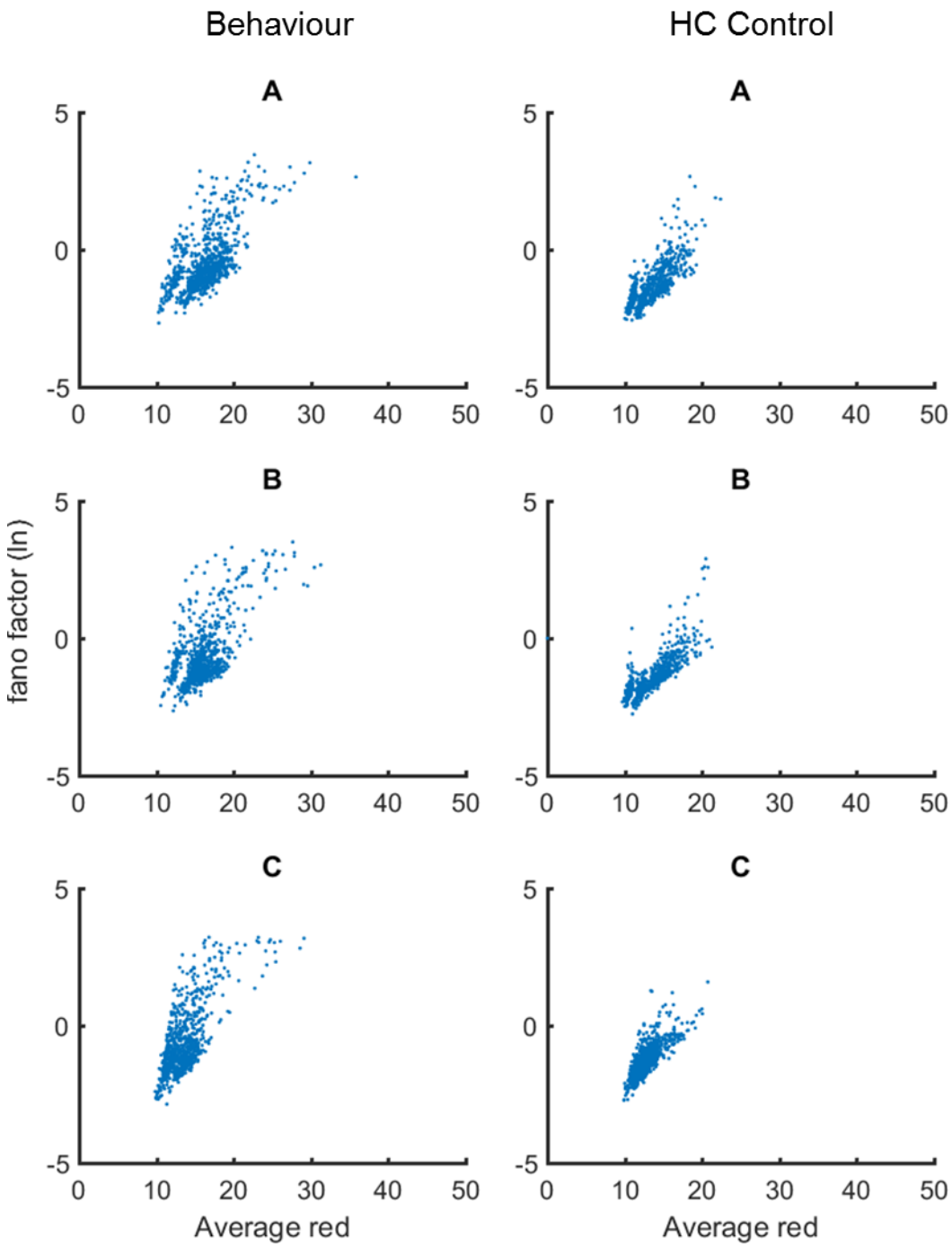

Figure 5.6a. Comparison of fano factor and average red values within nuclei at septotemporal positions A – C in behavioural and control groups.

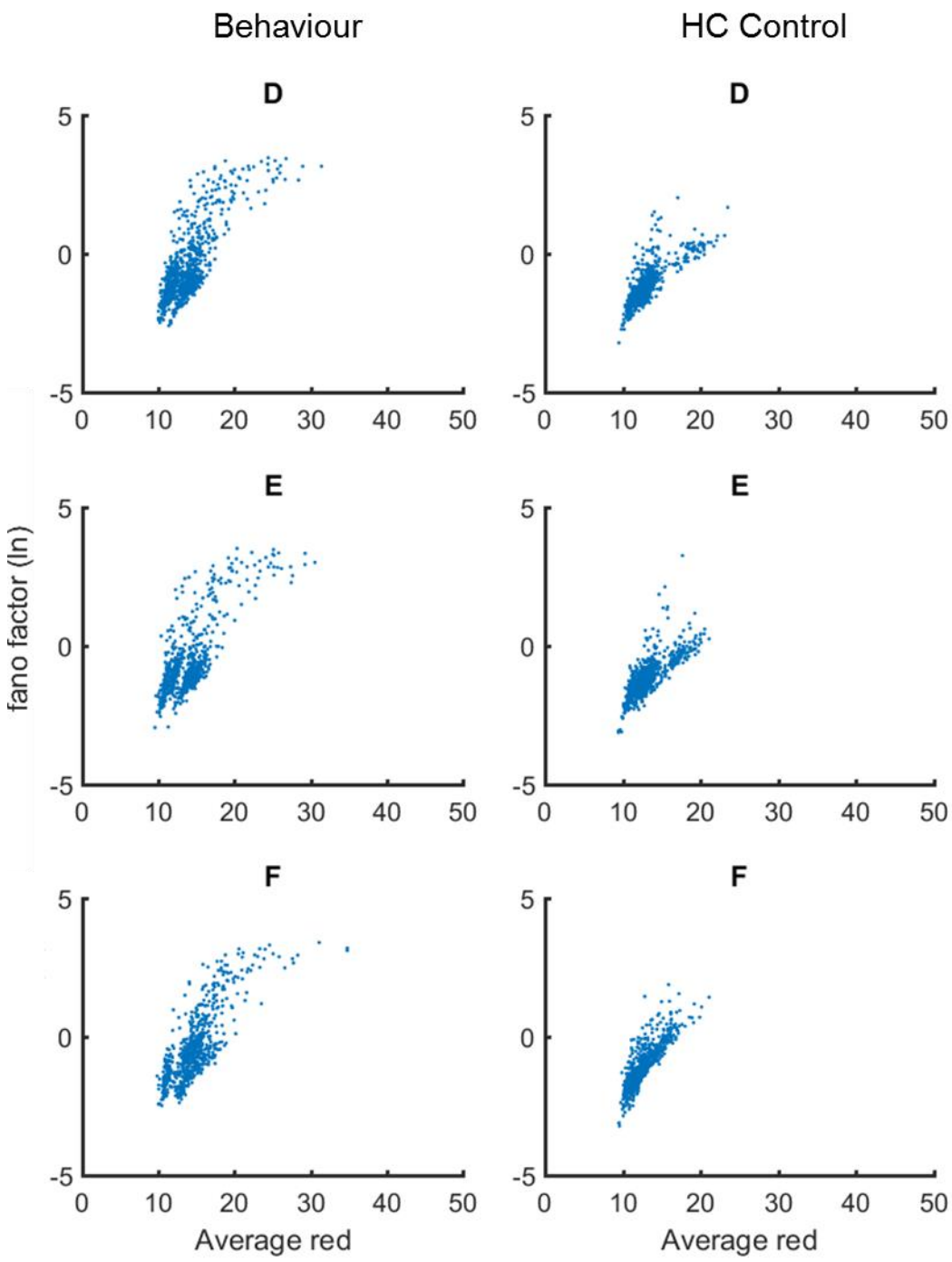

Figure 5.6b. Comparison of fano factor and average red values within nuclei at septotemporal positions D – F in behavioural and control groups.

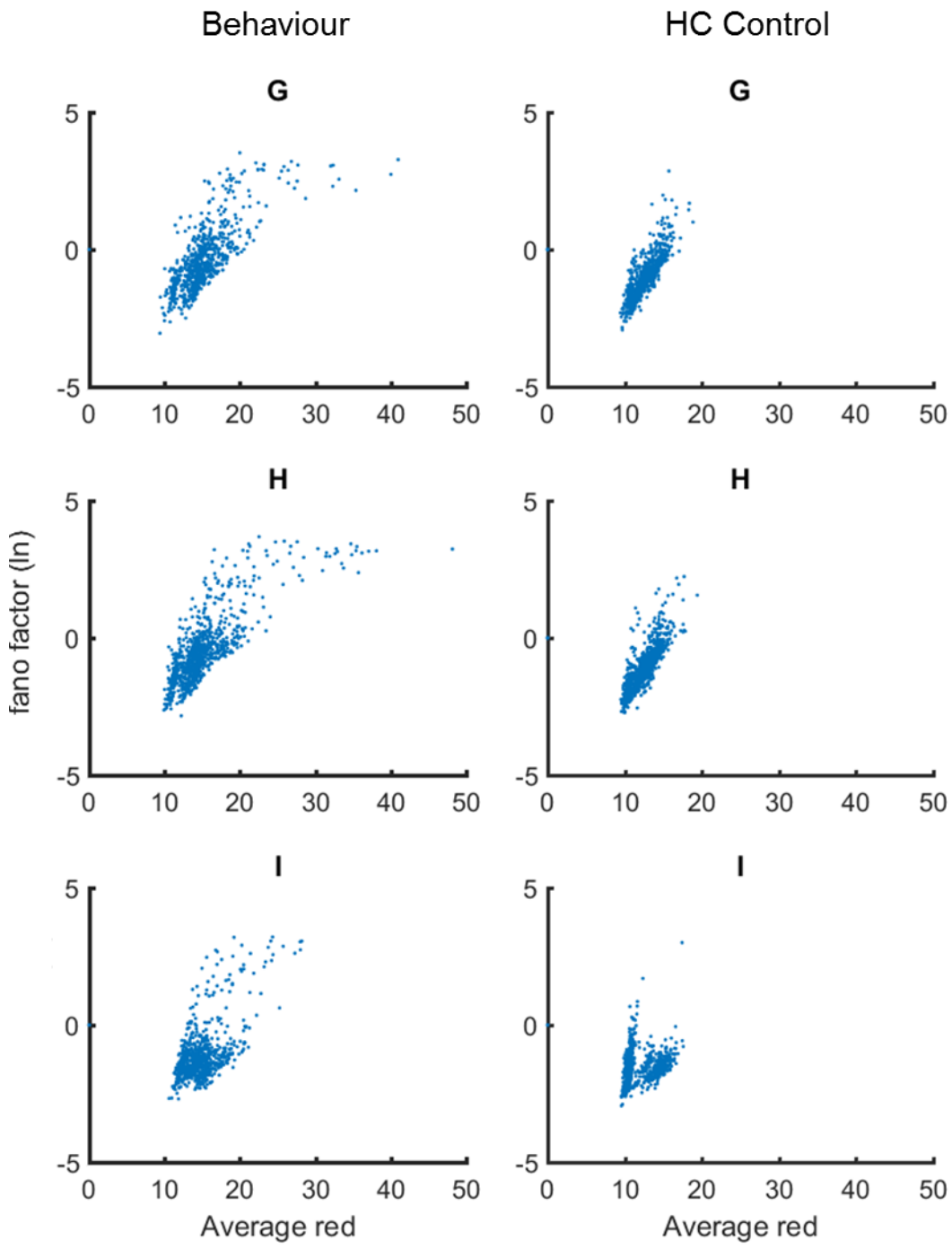

Figure 5.6c. Comparison of fano factor and average red values within nuclei at septotemporal positions G – I in behavioural and control groups.

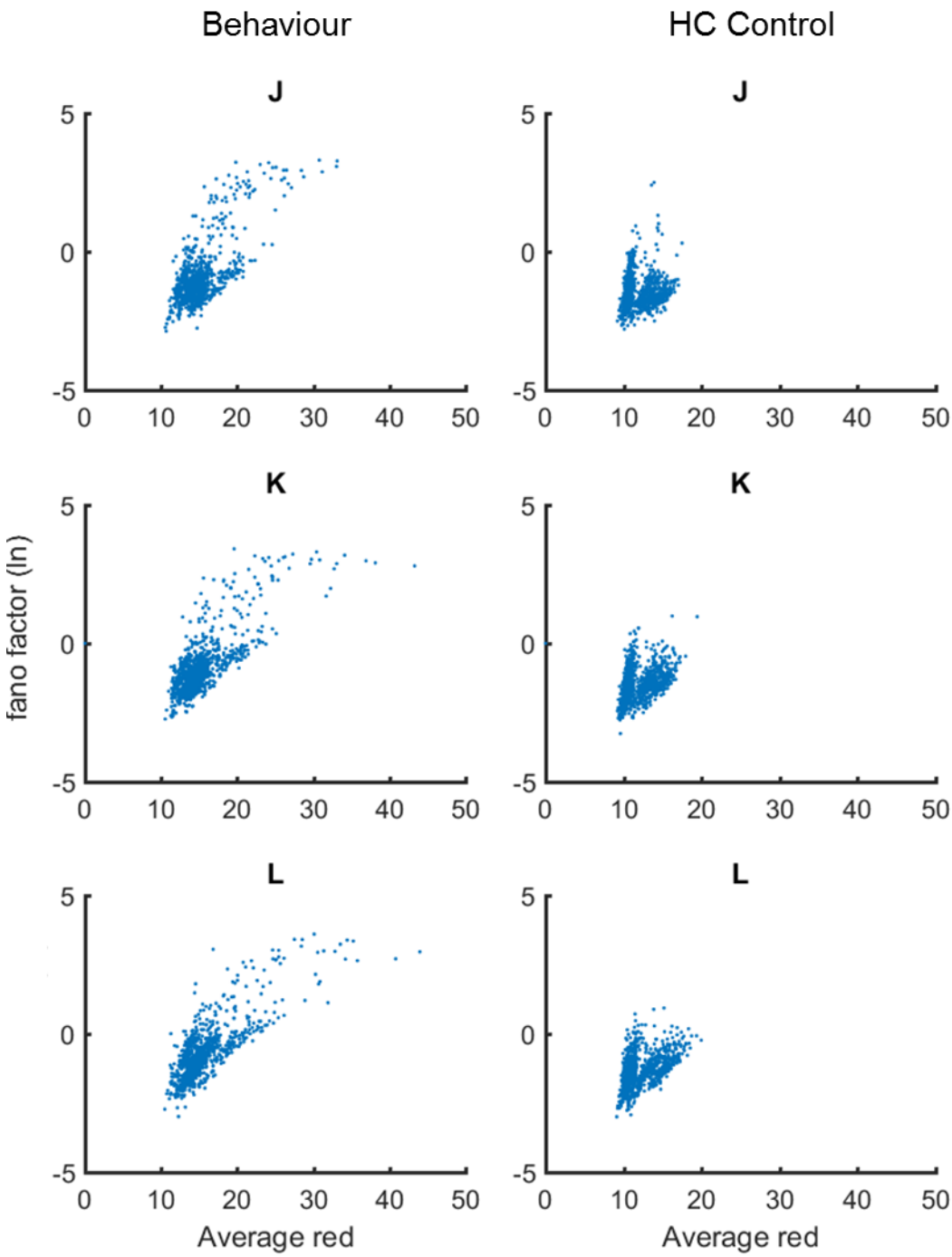

Figure 5.6d. Comparison of fano factor and average red values within nuclei at septotemporal positions J – L in behavioural and control groups.

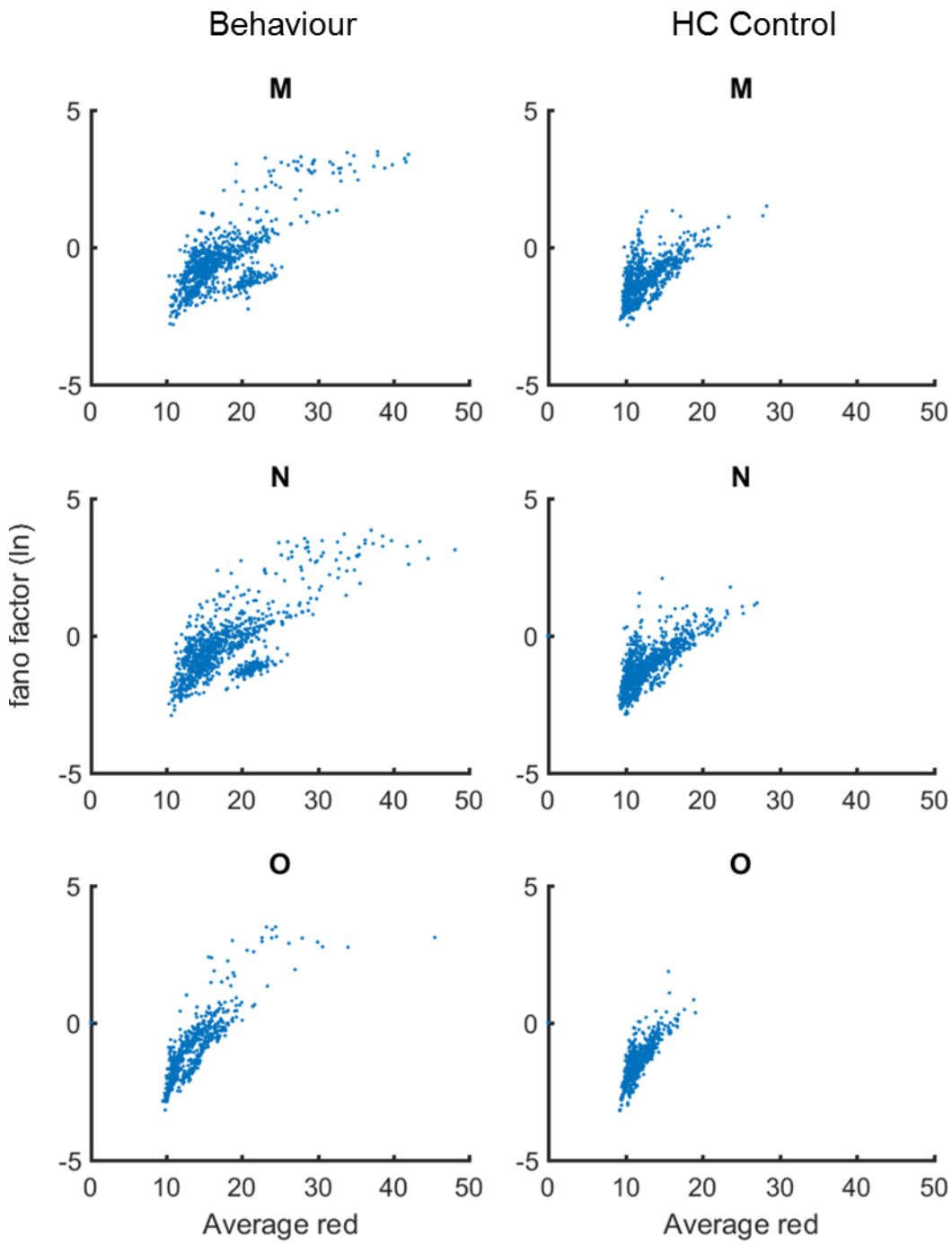

Figure 5.6e. Comparison of fano factor and average red values within nuclei at septotemporal positions M – O in behavioural and control groups.

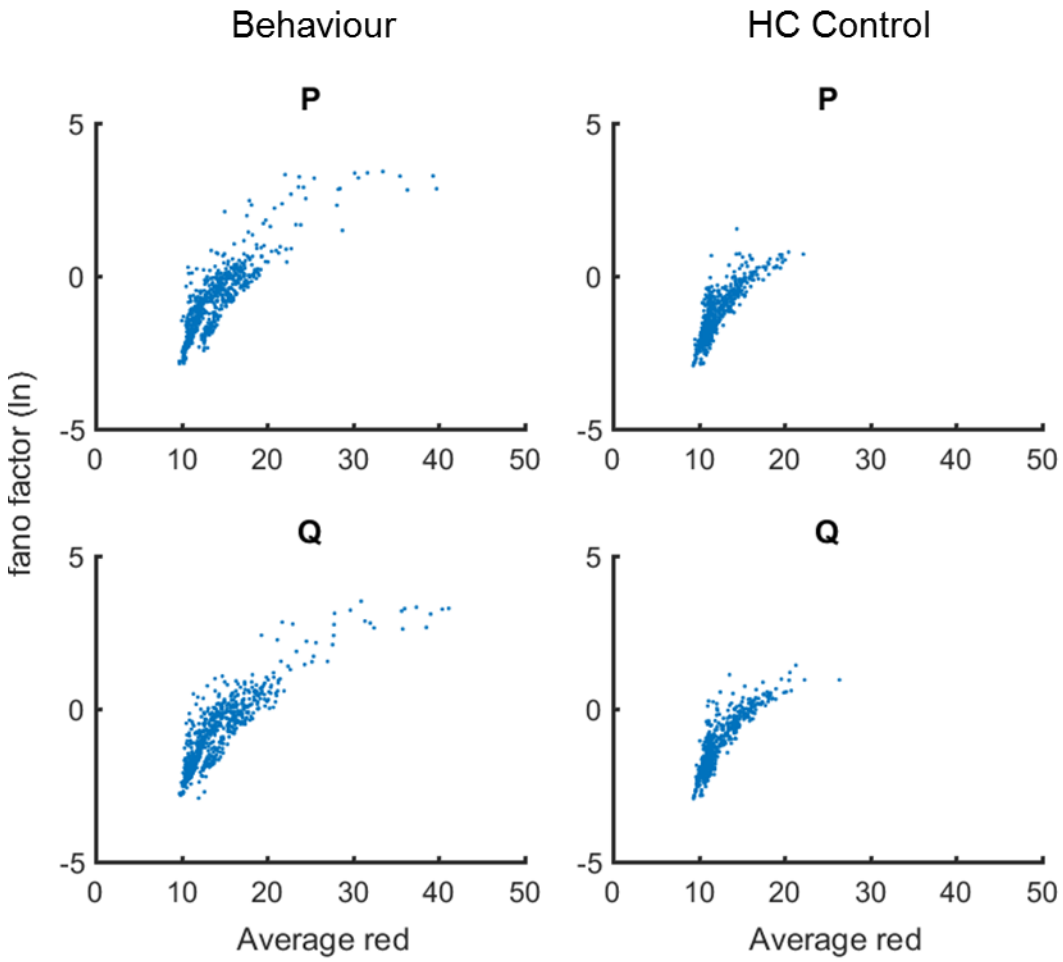

Figure 5.6f. Comparison of fano factor and average red values within nuclei at septotemporal positions P – Q in behavioural and control groups.

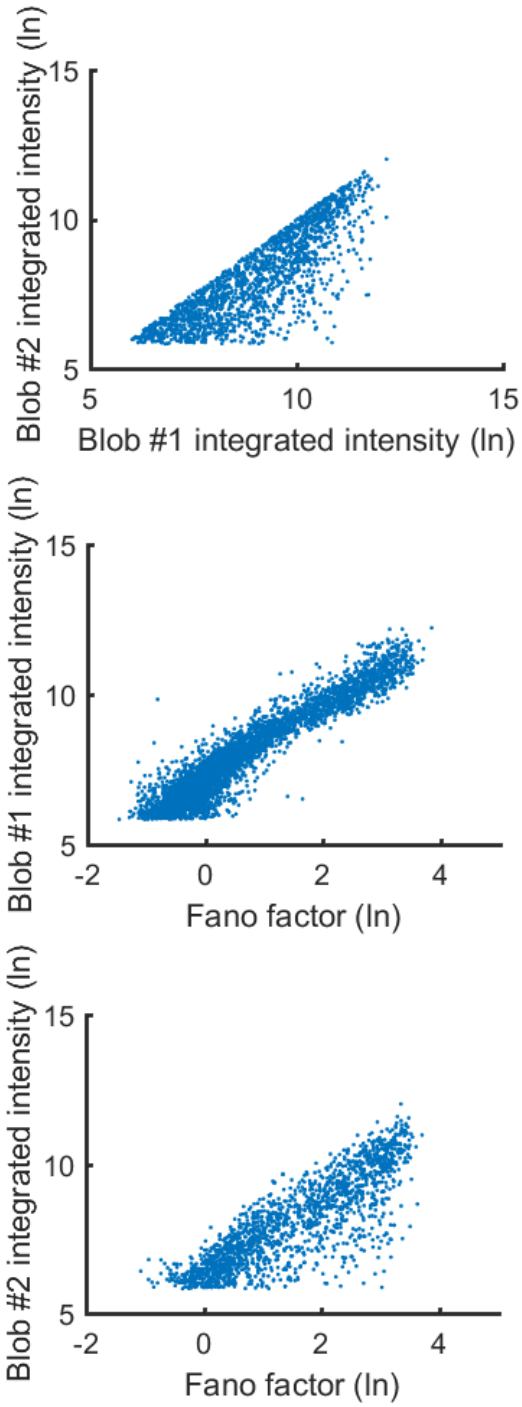

Figure 5.7. Comparison of fano factor and blob integrated intensity values. Top: comparison of total integrated intensity between blob1 and blob 2 within nuclei. Only data on nuclei containing two blobs are shown. Middle, bottom: Comparison of blob integrated intensity and fano factor value. Blob 1 was defined as the largest blob in the nucleus. Blob 1 vs fano factor are correlated ($p<0.0001$) Spearman $r = 0.9297$. Blob 2 vs fano factor are correlated ($p<0.0001$) Spearman $r = 0.08458$.